Supporting Information

for

Highly active superoxide dismutase mimic: pyridine-carboxamide based copper(II) complexes

*Róbert Diószegi[a], Andrea Guidetti[b], Norbert Ág[c], Ilenia Serra[b,d], Dóra Szalóki[e], Dóra Bonczidai-Kelemen[a], Nóra V. May[f], Erzsébet Fekete[c], Levente Karaffa[c], István Fábián[a,e], Sabine Van Doorslaer[b] *, Norbert Lihi[a,e] **

[a] Department of Inorganic and Analytical Chemistry, University of Debrecen, H-4032 Debrecen, Egyetem tér 1., Hungary

[b] Department of Chemistry, TSM[2] lab, University of Antwerp, Universiteitsplein 1, 2610 Antwerp, Belgium

c Department of Biochemical Engineering, University of Debrecen, H-4032 Debrecen, Egyetem tér 1., Hungary

[d] Laboratory of Bioenergetics and Protein Engineering, CNRS/AMU, Marseille, France

[e] HUN-REN–UD Mechanisms of Complex Homogeneous and Heterogeneous Chemical Reactions Research Group, University of Debrecen, H-4032 Debrecen, Egyetem tér 1., Hungary

[f] Centre for Structural Science, Research Centre for Natural Sciences, Hungarian Research Network (HUN-REN), Magyar tudósok körútja 2, H-1117 Budapest, Hungary

Corresponding authors: sabine.vandoorslaer@uantwerpen.be (S.V.D.), lihi.norbert@science.unideb.hu (N. L.)

TABLE OF CONTENTS

S1. Details of the synthesis

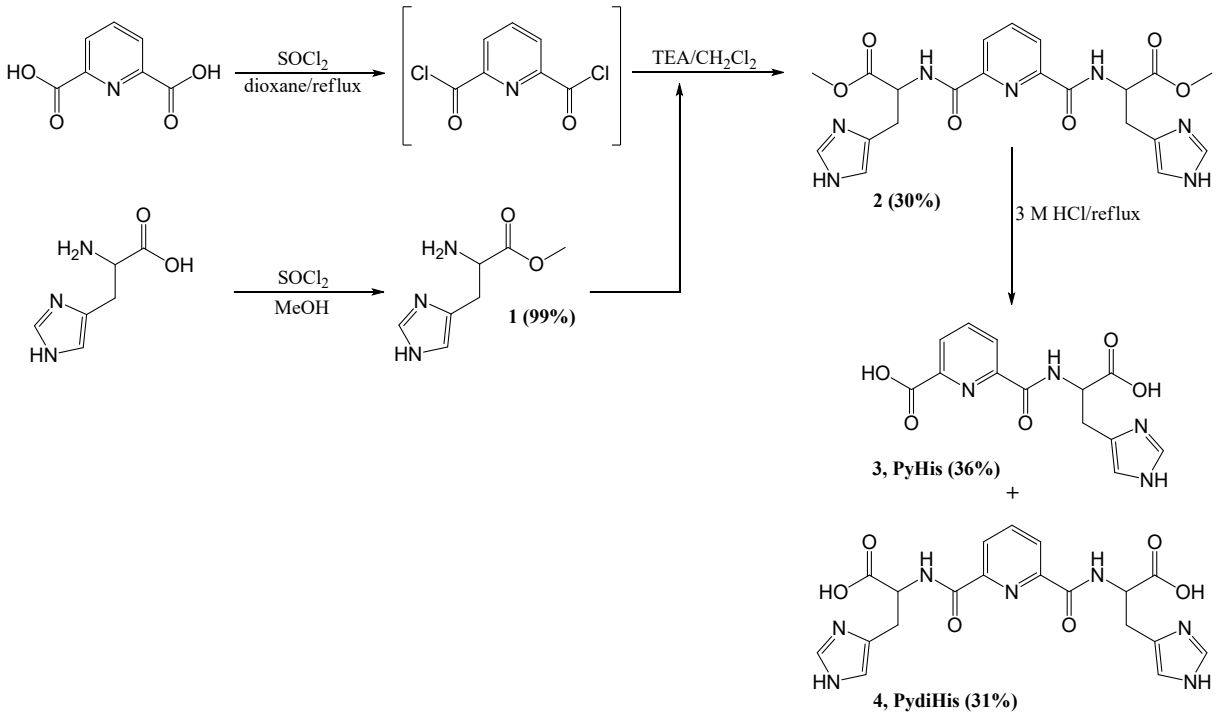

Scheme S1. Synthetic procedure of PyHis and PydiHis.

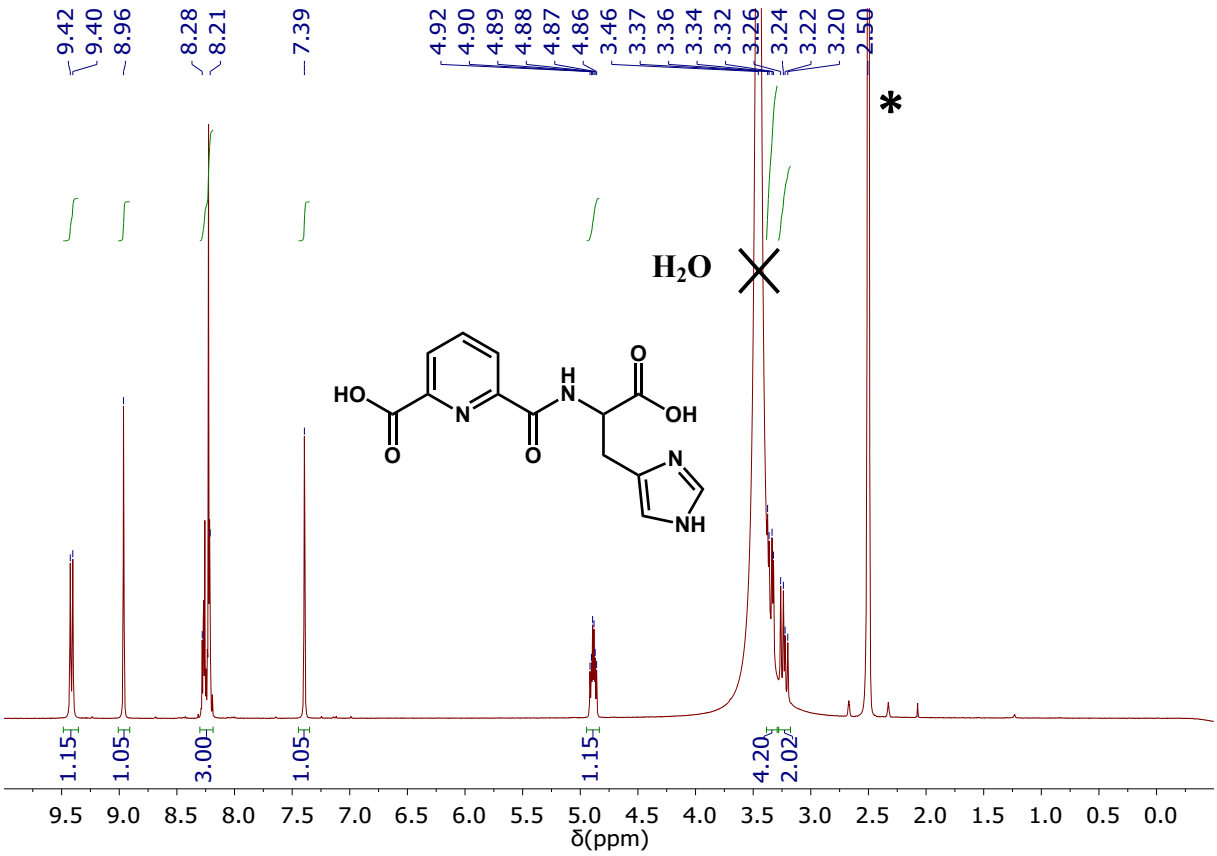

Figure S1. ^{1}H NMR (400 MHz) spectrum of PyHis in DMSO-d_6. The solvent residual peak is indicated by *.

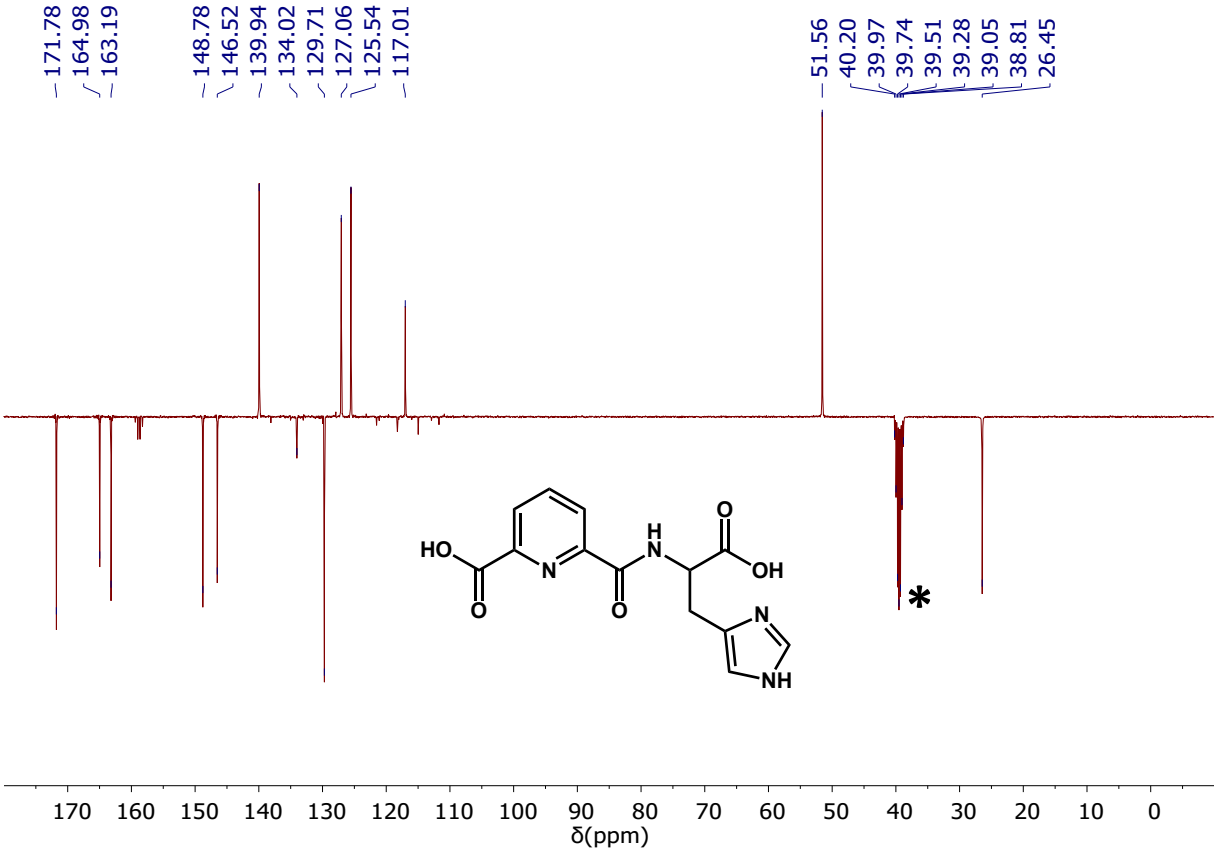

Figure S2. J-modulated ^{13}C NMR (90.5 MHz) spectrum of PyHis in DMSO-d_6. The solvent residual peak is indicated by *.

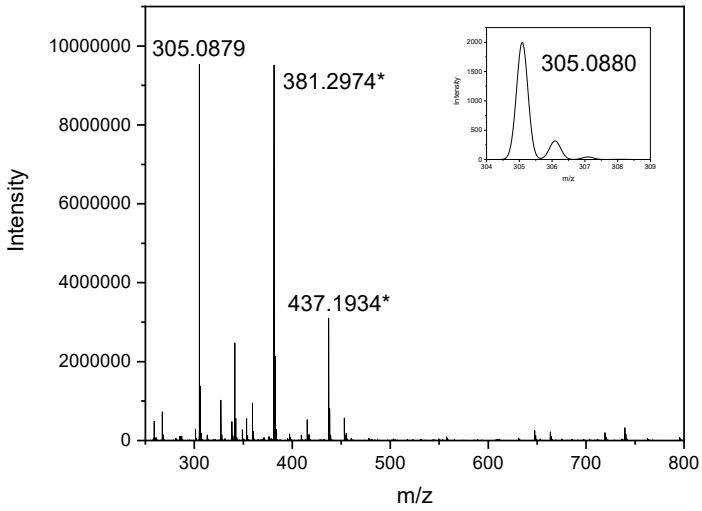

Figure S3. Mass spectrum of PyHis. Inset: Calculated isotope pattern of PyHis with $[C_{13}H_{13}N_4O_5]^+$ stoichiometry. Background peaks are indicated by *.

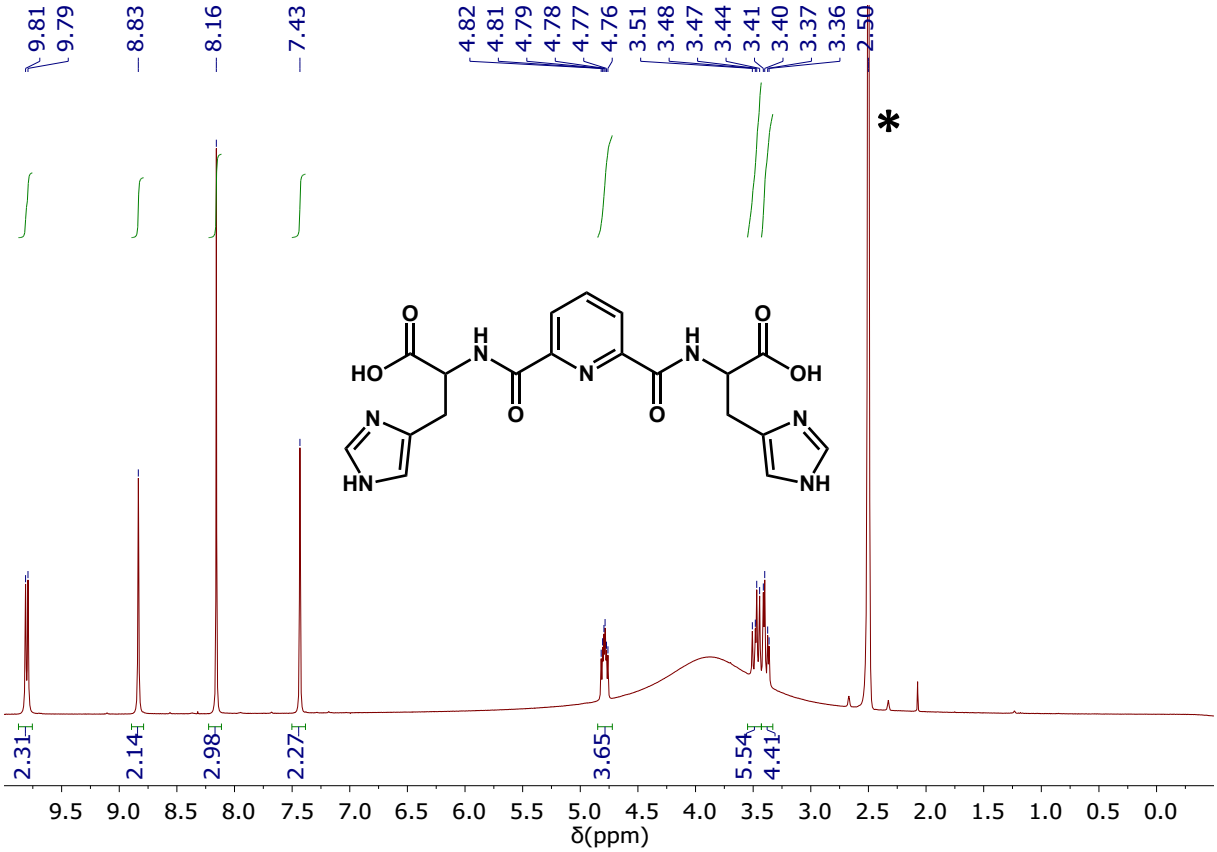

Figure S4. ^{1}H NMR (400 MHz) spectrum of PydiHis in DMSO-d_6. The solvent residual peak is indicated by *.

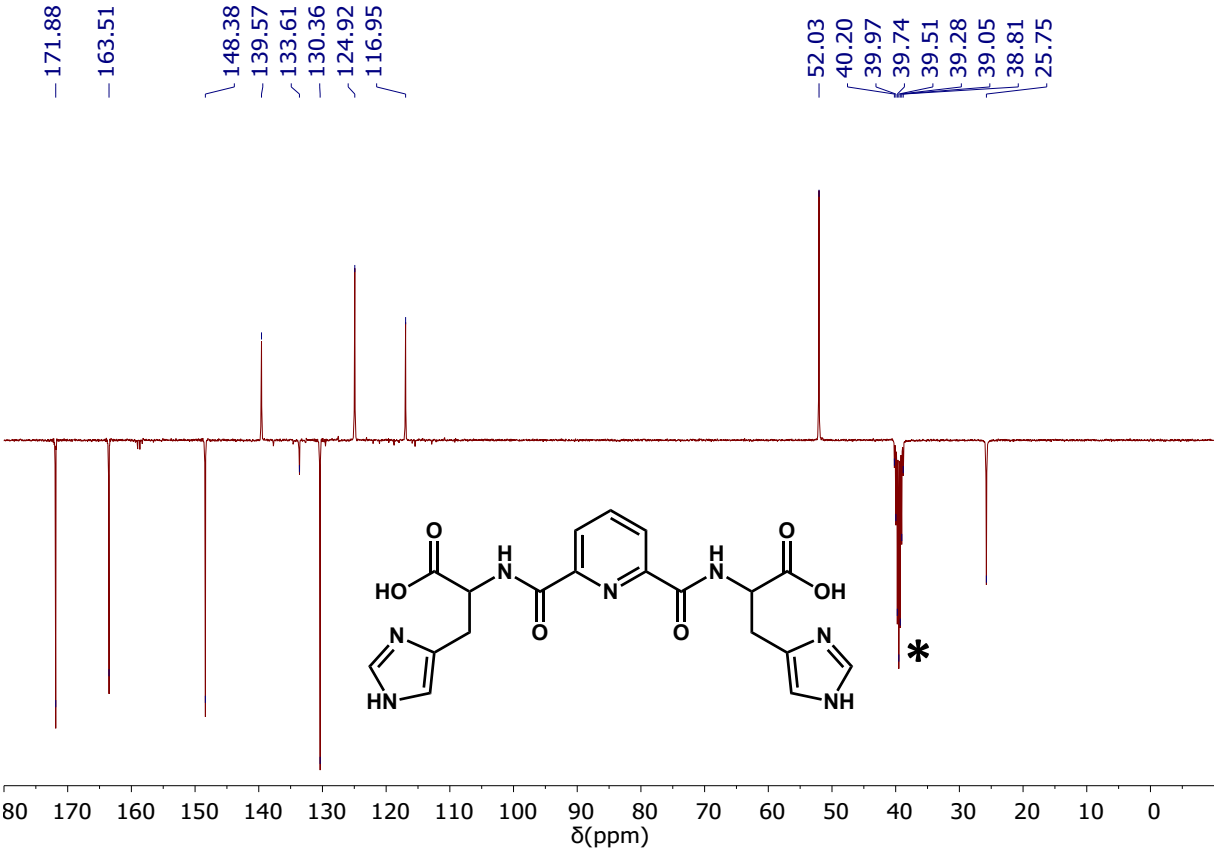

Figure S5. J-modulated ^{13}C NMR (90.5 MHz) spectrum of PydiHis in DMSO-d_6. The solvent residual peak is indicated by *.

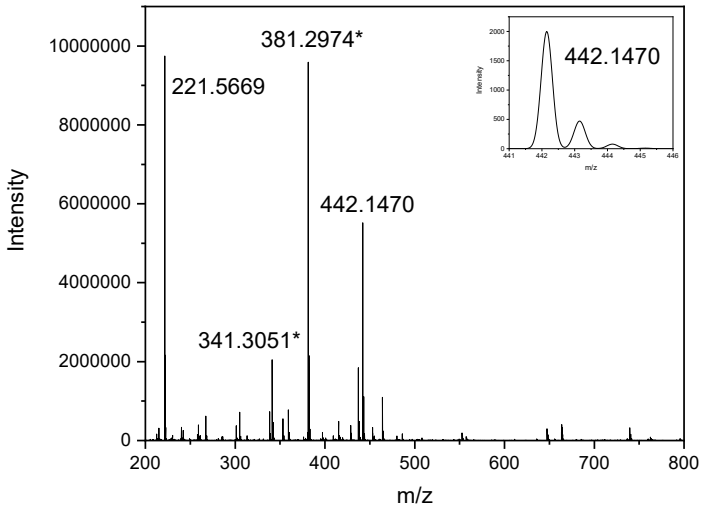

Figure S6. Mass spectrum of PydiHis. Inset: Calculated isotope pattern of PydiHis with $[C_{19}H_{20}N_7O_6]^+$ stoichiometry. Background peaks are indicated by *.

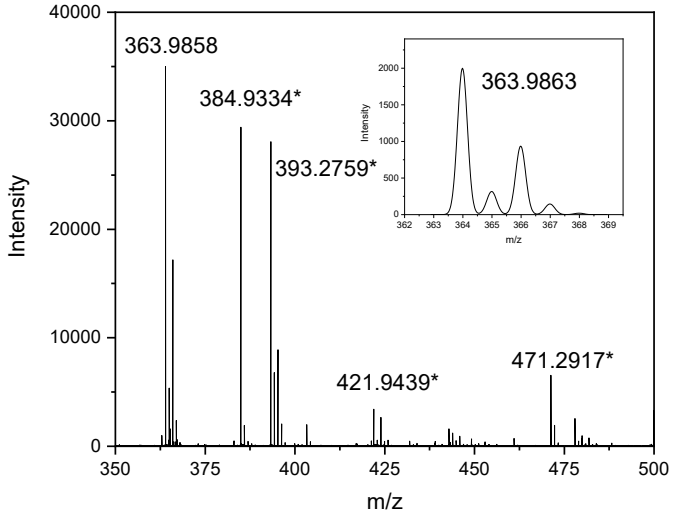

Figure S7. Mass spectrum of the copper(II) complex of PyHis. Inset: Calculated isotope pattern of the $[Cu(PyHisH_{-1})]^-$ complex with $[C_{13}H_9N_4O_5Cu]^-$ stoichiometry. Background peaks are indicated by *.

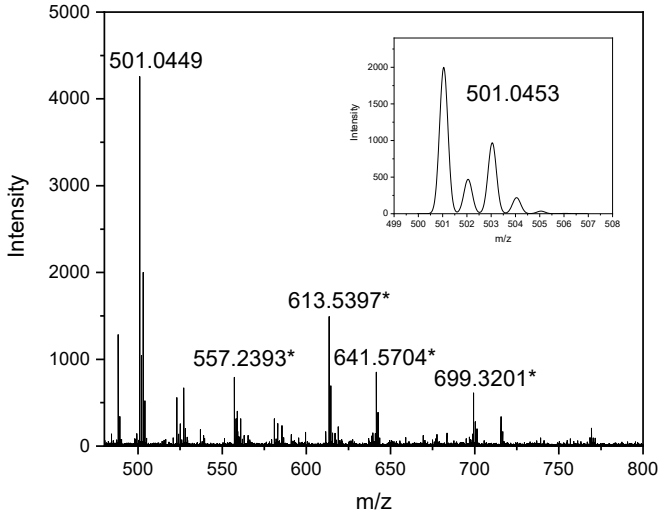

Figure S8. Mass spectrum of the copper(II) complex of PydiHis. Inset: Calculated isotope pattern of the $[Cu(PydiHisH_{-1})]^-$ complex with $[C_{19}H_{16}N_7O_6Cu]^-$ stoichiometry. Background peaks are indicated by *.

S2. Acid-base equilibria

The acid dissociation constants (pK_a) of the ligands were determined by pH-potentiometric titrations and the results are reported in Table S1 along with the corresponding pK_a-s values reported for the pyridine-2,6-dicarboxilic acid.[1]

In principle, the pyridinium group of the pyridine-2,6-dicarboxamide platform, the carboxylate groups as well as the imidazolium ion of histidine residue(s) can be involved in acid-base processes (Scheme 1). However, one less than all possible acid dissociation constants could be determined based on the potentiometric titrations, i.e., only 4 and 3 pK_a-s for PydiHis and PyHis, respectively. It is reasonable to assume that the deprotonation of one of the carboxylate groups or the pyridinium group is outside the potentiometrically measurable pH-range. To identify the protonation sites, pH-dependent ^{1}H NMR spectra were recorded. Relevant sections of the NMR spectra of PyHis and PydiHis are shown in Figure S9 and S10 and the normalized chemical shifts as a function of pH are shown in Figure S11. A drastic pH effect was observed on the peaks of the aromatic imidazole hydrogens in the pH range 6 – 8 due to the protonation of the imidazole-N. The peaks of the β-hydrogen of histidine shift as a function of pH in the entire studied pH range indicating that the protolytic equilibria of both the imidazole ring and the carboxylic group have an impact on the chemical environment of these hydrogens. In the case of PydiHis, the signals of the aromatic pyridine hydrogens do not exhibit any pH dependence. This leads to the conclusion that the protonation of the pyridine-N does not occur in the potentiometrically accessible pH range, and the determined pK_a-s are assigned to the acid – base equilibria of the carboxylic groups and the histidine residues. Presumably the same applies to PyHis, where one of the carboxylate groups is directly connected to the pyridine ring, and the corresponding protonation equilibrium has a small impact on the chemical shift of the aromatic hydrogen peaks.

Table S1. Acid dissociation constants (pK_a) of PyHis, PydiHis and

pyridine-2,6-dicarboxilic acid (T = 25°C and I = 0.2 M KCl)

	PyHis	PydiHis	pyridine-2,6-dicarboxilic acid [a]
pK_{a1}	2.48 ± 0.03	2.10 ± 0.02	0.52
pK_{a2}	3.18 ± 0.04	2.99 ± 0.04	2.03
pK_{a3}	7.11 ± 0.03	6.77 ± 0.03	4.49
pK_{a4}		7.58 ± 0.04	

[a] Data are taken from Ref. [1].

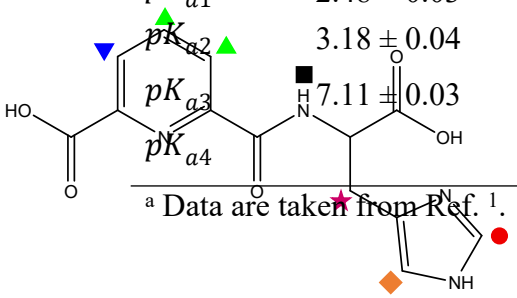

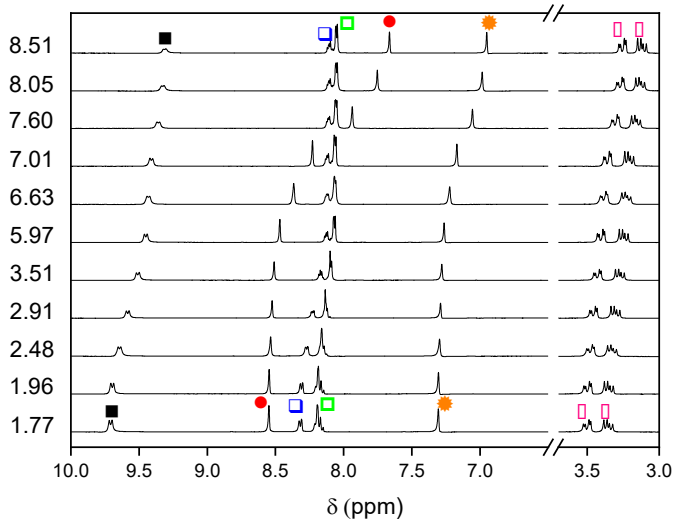

Figure S9. Selected part of the ^{1}H NMR spectra of PyHis as a function of pH and the assignment of ^{1}H NMR signals.

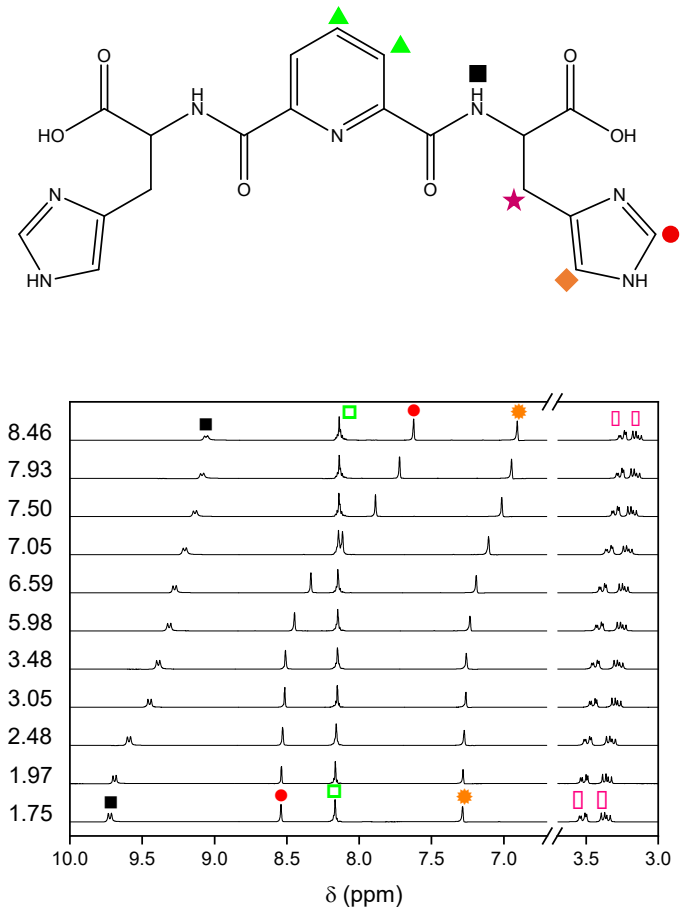

Figure S10. Selected part of the ^{1}H NMR spectra of PydiHis as a function of pH and the assignment of ^{1}H NMR signals.

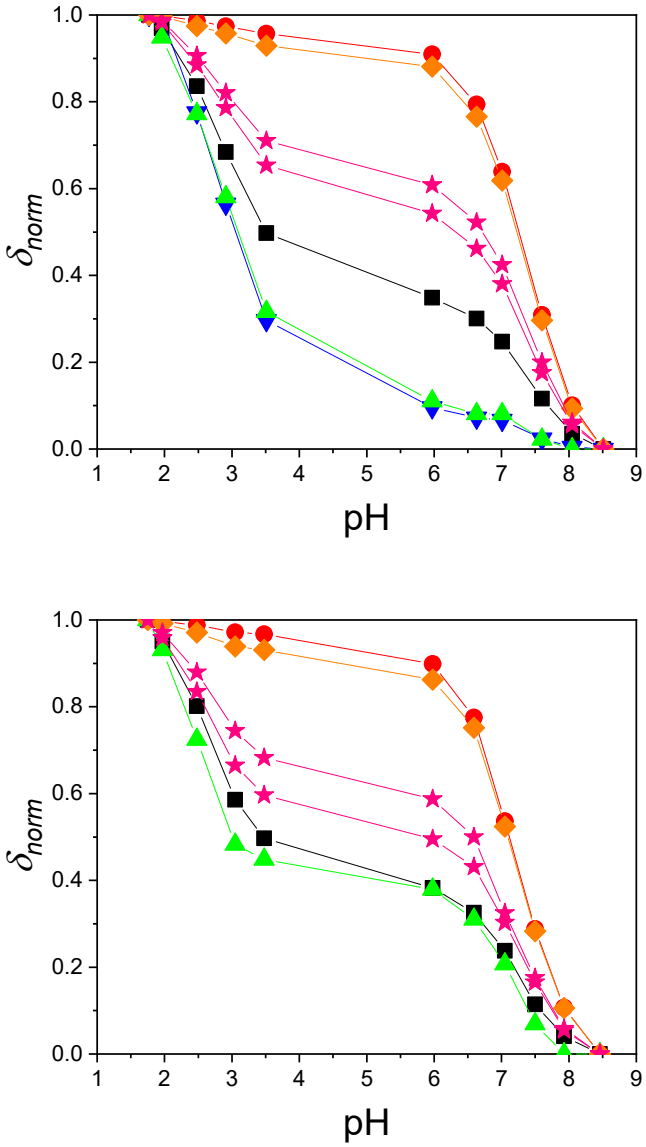

Figure S11. Normalized ^{1}H chemical shift variation of PyHis (top) and PydiHis (bottom) as a function of pH. NMR assignment of the ligands is provided in Figure S9-10. c_{PyHis} = 8.02 mM, c_{PydiHis} = 8.10 mM.

S3. UV-Vis and CW-EPR data of the Cu(II)/PyHis system

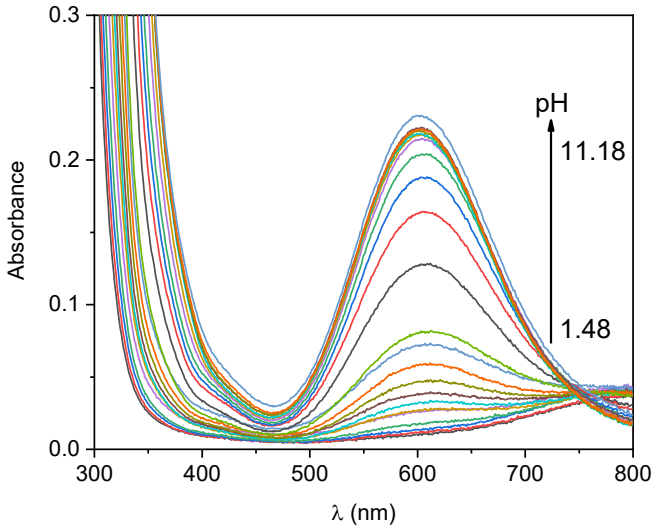

Figure S12. pH-dependent UV-Vis spectra for Cu(II)/PyHis 1:1 system. c_{Cu} = 1.72 mM.

Table S2. Isotropic and anisotropic *g* and copper hyperfine parameters of the complexes determined by the simulation of the room temperature and frozen solution EPR spectra recorded in the Cu(II) - PyHis and Cu(II) - PydiHis systems.[a] The relative signs of the copper hyperfine principal values are derived assuming a negative isotropic value as confirmed by DFT and knowing that the isotropic value is the average of the three principal components. The data are used for the simulations of Figures S13-S15.

	Isotropic EPR paramteres		**Anisotropic EPR parameters**						**Calculated isotropic EPR parameters**[b]
Cu(II) - PyHis									
	g_0	A_0 (MHz)	g_x	g_y	g_z	A_x (MHz)	A_y (MHz)	A_z (MHz)	$g_{o,calc}$[b]
[CuL]	n.d.	n.d.	2.072	2.072	2.363	21.5	21.5	-453.1	2.169
$[CuLH_{-1}]^{-}$[c]	2.1075	-176.4	2.038	2.060	2.219	-59.3	8.6	-514.9	2.106
$[CuL_2]^{2-}$	2.1529	-94.3	2.293	2.181	2.014	165.0	-132.8	-365.6	2.162
Cu(II) - PydiHis									
	g_0	A_0 (MHz)	g_x	g_y	g_z	A_x (MHz)	A_y (MHz)	A_z (MHz)	g_o
$[CuLH]^{+}$	n.d.	n.d.	2.065	2.065	2.361	44.5	44.5	-441.2	2.164
[CuL]	2.112	-158.7	2.055	2.055	2.225	64.7	-64.7	-521.9	2.112
$[CuLH_{-1}]^{-}$[d]	2.113	-205.8	2.049	2.049	2.229	-49.6	-49.6	-553.5	2.109
$[CuLH_{-2}]^{2-}$	2.117	-175.7	2.020	2.104	2.213	123.6	-151.7	-460.3	2.112

[a]The experimental error was ±0.002 for g_x and g_y; ±0.001 for g_z; ± 0.1 MHz for A_x and A_y; ±0.2 MHz for A_z couplings. [b] Calculated by the equation $g_{0,calc} = (g_x+g_y+g_z)/3$. [c] Isotropic nitrogen couplings of a_0^{N1} = 0.9 mT and twice a_0^{N2} = 1.5 mT were taking into account in the simulation of room temperature spectra and anisotropic nitrogen couplings of a_x^{N1}=1.5 mT, a_y^{N1}=a_z^{N1}=1.0 mT and two equivalent a_y^{N2}=1.8 mT, a_x^{N2}=a_z^{N2}=1.0 mT were taking into account in the simulation of frozen solution spectra. [d] Isotropic nitrogen couplings of 2 nitrogen nuclei with a_0^{N} = 1.4 mT, 2 with a_0^{N} =1.2 mT were taking into account in the simulation of room temperature spectra.

Table S3. Calculated component ratios (%) obtained from the simulation of room temperature and frozen solution CW-EPR experiments (Figure S13, S14)

Cu(II)/PyHis 1:1 room temperature

pH	Cu^{2+}	[Cu(PyHis)]	$[Cu(PyHisH_{-1})]^{-}$	$[Cu(PyHis)_2]^{2-}$
2.99	0	0	100	0
4.00	0	0	100	0
7.70	0	0	100	0
10.16	0	0	100	0

Cu(II)/PyHis 1:1 frozen solution

pH	Cu^{2+}	[Cu(PyHis)]	$[Cu(PyHisH_{-1})]^{-}$	$[Cu(PyHis)_2]^{2-}$
2.99	0	0	90	10
4.00	0	0	100	0
7.70	0	0	100	0
10.16	0	0	100	0

Cu(II)/PyHis 1:2 room temperature

pH	Cu^{2+}	[Cu(PyHis)]	$[Cu(PyHisH_{-1})]^{-}$	$[Cu(PyHis)_2]^{2-}$
1.63	40	0	25	35
2.90	0	0	86	14
4.42	0	0	100	0
6.17	0	0	100	0
10.11	0	0	100	0

Cu(II)/PyHis 1:2 frozen solution

pH	Cu^{2+}	[Cu(PyHis)]	$[Cu(PyHisH_{-1})]^{-}$	$[Cu(PyHis)_2]^{2-}$
1.63	28	64	0	8
2.90	0	0	54	46
4.42	0	0	100	0
6.17	0	0	100	0
10.11	0	0	100	0

Cu(II)/PyHis 1:8 frozen solution

pH	Cu^{2+}	[Cu(PyHis)]	$[Cu(PyHisH_{-1})]^{-}$	$[Cu(PyHis)_2]^{2-}$
3.00	0	0	23	77

Cu(II)/PydiHis 1:1 room temperature

pH	Cu^{2+}	$[Cu(H(PydiHis))]^{+}$	[Cu(PydiHis)]	$[Cu(PydiHisH_{-1})]^{-}$	$[Cu(PydiHisH_{-2})]^{2-}$
3.02	75	0	25	0	0
4.11	8	0	60	32	0
4.93	0	0	20	80	0
6.89	0	0	0	100	0
7.51	0	0	0	100	0
10.88	0	0	0	0	100
11.50	0	0	0	0	100

Cu(II)/PydiHis 1:1 frozen solution

pH	Cu^{2+}	$[Cu(H(PydiHis))]^{+}$	[Cu(PydiHis)]	$[Cu(PydiHisH_{-1})]^{-}$	$[Cu(PydiHisH_{-2})]^{2-}$
3.02	70	23	7	0	0
4.11	0	12	88	0	0
4.93	0	0	64	36	0
6.89	0	0	0	100	0
7.51	0	0	0	100	0
10.88	0	0	0	0	100
11.50	0	0	0	0	100

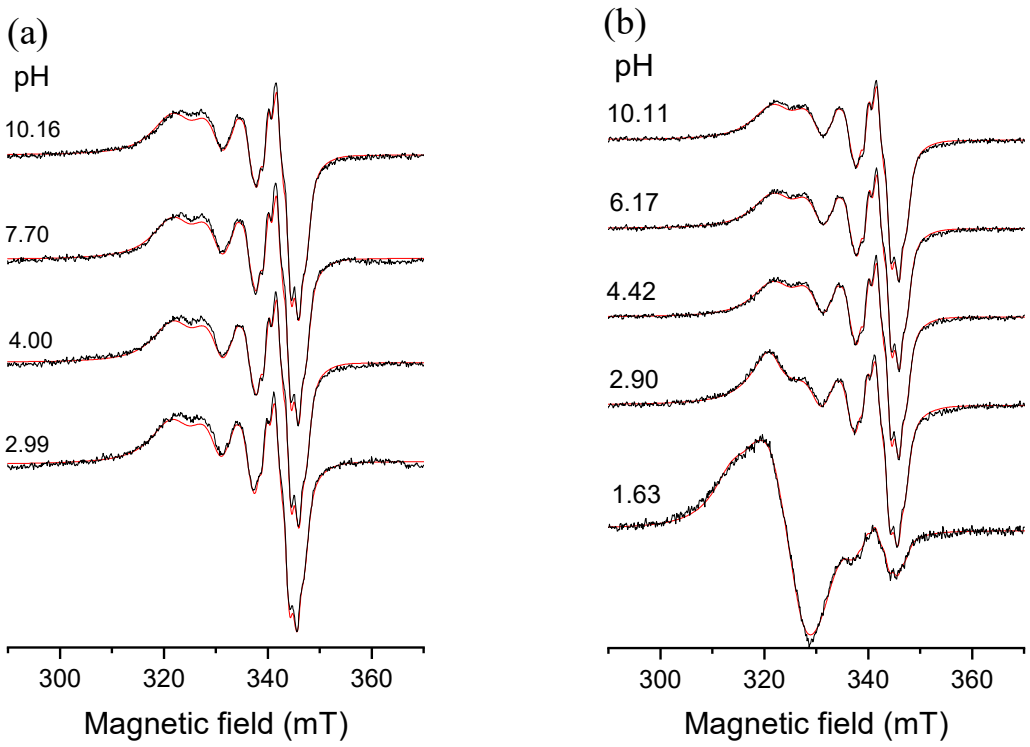

Figure S13. pH dependent experimental (black) and simulated (red) solution EPR spectra recorded for the Cu(II)–PyHis at concentration (a) $c_L = c_{Cu} = 1.90$ mM and (b) $c_{Cu} = 1.90$ mM and $c_L = 4.00$ mM in aqueous solution at 295 K.

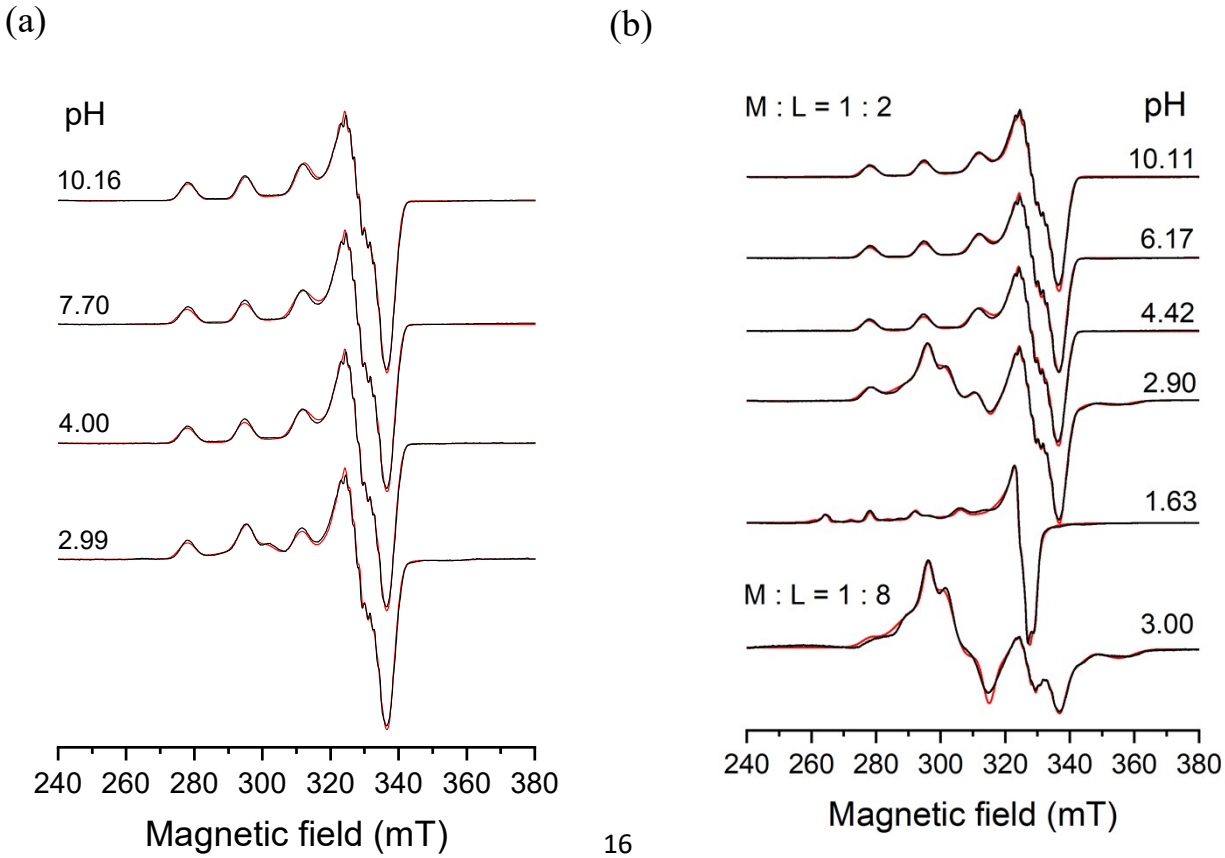

Figure S14. pH dependent experimental (black) and simulated (red) solution EPR spectra recorded for the Cu(II)–PyHis at equimolar solution (a) $c_L = c_{Cu} = 1.90$ mM and ligand excess (b) $c_{Cu} = 1.90$ mM and $c_L = 4.00$ mM and $c_{Cu} = 1.00$ mM and $c_L = 8.00$ mM in frozen solution at 77K.

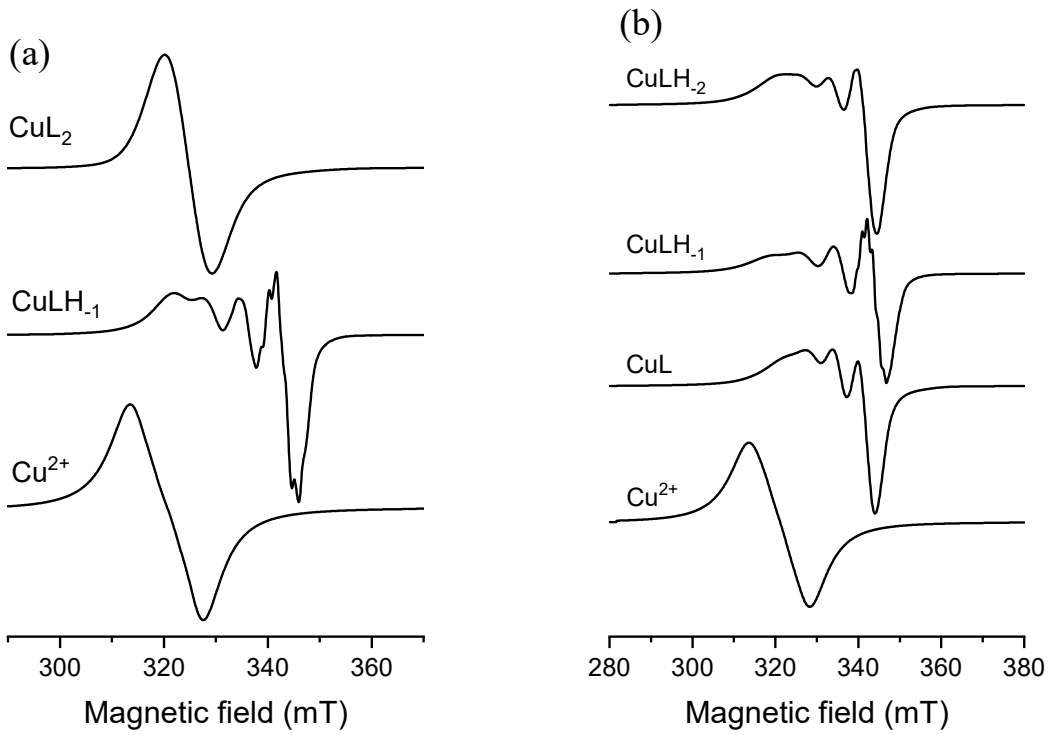

Figure S15. Calculated components contributing to the room-temperature CW-EPR spectra for the Cu(II)-PyHis (a) and Cu(II)-PydiHis (b) complexes.

S4. Complex formation processes in the Cu(II) and PyHis system at 1:2 metal ion-to-ligand ratio

When PyHis was applied in excess relative to the copper(II) ion, $[Cu(PyHis)_2]^{2-}$ forms at pH ~ 3 (Figure S14b). By increasing the pH, the copper(II)-induced ionization and coordination of carboxamide nitrogen yields the $[Cu(PyHisH_{-1})(H_2O)]^{-}$ complex which indicates that copper(II) favors the (O,3N) donor set with its (5,5,6)-membered joined chelate system. Indeed, EPR spectra do not show the formation of further bis complexes (Figures S13, S14).

$[Cu(PyHis)_2]^{2-}$ features an unusual CW-EPR spectrum with high rhombicity of the ***g*** tensor. For complexes of this type, parameter $R = (g_2-g_3)/(g_1-g_2)$ where $g_1 > g_2 > g_3$ can be indicative for the predominance of the d_{z^2} or $d_{x^2-y^2}$ orbital in the ground state.[2]

The greater contribution to the ground state arises from the d_z^2 or the $d_{x^2-y^2}$ orbital when $R > 1$ and $R < 1$, respectively. For $[Cu(PyHis)_2]^{2-}$, the R value is 1.48, indicating an inverse spectrum with g values $g_x > g_y > g_z > 2.0023$, where greater contribution to the ground state arises from the d_{z^2} orbital. This indicates a compressed octahedral geometry. This structure can be envisioned when two shorter axial bonds from the two pyridine nitrogen atoms are accommodated in the coordination sphere of copper(II), while two carboxylate groups and two imidazole nitrogen atoms coordinate equatorially with longer bonds (Figure S16). Such inverse copper(II) EPR spectra were reported in the case of the ternary copper(II) complexes of 2,6-pyridinedimethanol and chlorosalicylic acid.[3]

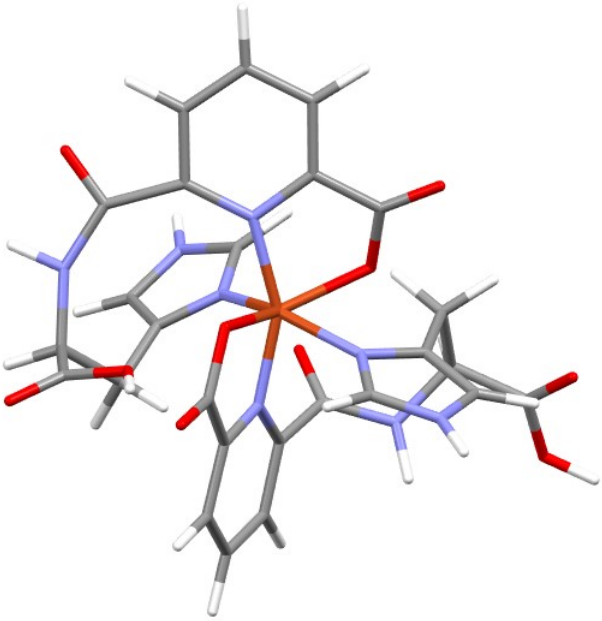

Figure S16. Proposed coordination mode of $[Cu(PyHis)_2]^{2-}$.

S5. XRD data

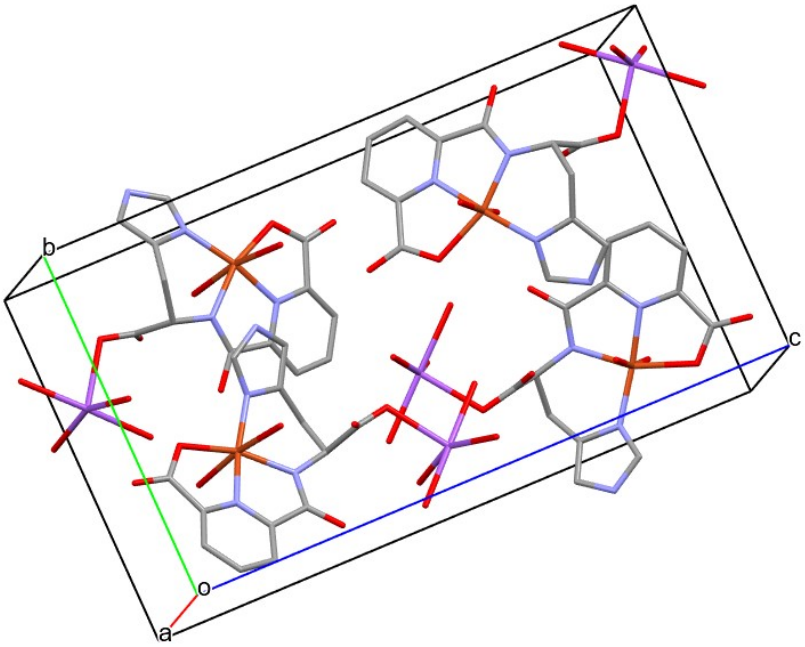

Figure S17. Unit cell of crystal, $[Cu(PyHisH_{-1})(H_2O)_2Na(H_2O)_4]$.

Table S4. Crystal data and structure refinement.

Empirical formula	$C_{21}H_{23}N_3O_2$
Moiety formula	C13 H21 Cu N4 Na O11
Formula weight	495.87
Temperature (K)	143(2)
Radiation and wavelength (Å)	Mo-Kα, 0.71073
Crystal system	orthorhombic
Space group	$P2_12_12_1$
Unit cell dimensions	
*a (*Å)	7.4853(2)
b (Å)	11.9169(4)
c (Å)	20.9139(7)
α (°)	90°
β (°)	90°
γ (°)	90°
Volume (Å^3)	1865.55(10)
Z/Z'	4/1
Density (calculated) (Mg/m^3)	1.765
Absorption coefficient, μ (mm^{-1})	1.264
F(000)	1020
Crystal colour	blue
Crystal description	block
Crystal size (mm)	0.50 x 0.50 x 0.10
Absorption correction	numerical
Max. and min. transmission	0.907, 0.969
θ–range for data collection (°)	$3.214 \leq \theta \leq 27.438$
Index ranges	$-9 \leq h \leq 9$; $-15 \leq k \leq 15$; $-27 \leq l \leq 27$
Reflections collected	53605
Completeness to 2θ	0.998
Independent reflections (R_{int})	4256 (0.0530)
Reflections $I>2\sigma(I)$	4113
Refinement method	full-matrix least-squares on F^2
Data / restraints / parameters	4256 /0 /278
Goodness-of-fit on *F*2	1.155
Final *R* indices [$I>2\sigma(I)$] (R1, wR2)	0.0315, 0.0645
R indices (all data) (R1, wR2)	0.0338, 0.0652
Max. and mean shift/esd	0.001;0.000
Largest diff. peak and hole (e.Å^{-3})	0.360;-0.417 e.Å^{-3}

Table S5. Selected bond lengths (Å) and angles (°) for crystal [Cu(PyHisH$_{-1}$)(H$_2$O)$_2$Na(H$_2$O)$_4$].

Cu1-N1	1.920(3)	Cu1-N3	1.944(3)
Cu1-N2	1.985(3)	Cu1-O1	2.089(2)
Cu1-O7	2.759(2)	Cu1-O6	2.477(3)
Na1-O5	2.342(2)	Na1-O10	2.366(3)
Na1-O11	2.364(3)	Na1-O8	2.366(2)
Na1-O9	2.333(3)	O2-C6	1.239(4)
O3-C7	1.268(4)	O5-C13	1.260(4)
O4-C13	1.262(4)	O1-C6	1.286(4)
N1-C1	1.329(4)	N1-C5	1.331(4)
N3-C12	1.326(4)	N3-C10	1.387(4)
N4-C12	1.338(4)	N4-C11	1.366(4)
N2-C7	1.317(4)	N2-C8	1.456(4)
C5-C4	1.384(4)	C5-C7	1.512(4)
C13-C8	1.535(4)	C13-Na1	3.089(3)
C9-C10	1.493(4)	C9-C8	1.550(4)
C1-C2	1.391(5)	C1-C6	1.516(5)
C4-C3	1.395(5)	C10-C11	1.366(4)
C2-C3	1.390(5)	O10-Na1#1	2.366(3)

N1-Cu1-N3	168.0(1)	N1-Cu1-N2	81.0(1)
N3-Cu1-N2	95.3(1)	N1-Cu1-O1	79.0(1)
N3-Cu1-O1	103.4(1)	N2-Cu1-O1	159.7(1)
O7-Cu1-O1	91.8(1)	O9-Cu1-O6	170.9(1)
O7-Cu1-N3	88.2(1)	O7-Cu1-N2	80.7(1)
O5-Na1-O10	83.6(1)	O11-Na1-O8	84.5(1)
O5-Na1-O8	95.7(1)	O11-Na1-O9	154.8(1)
O5-Na1-O9	89.9(1)	O10-Na1-O8	174.3(1)
O11-Na1-O10	90.6(1)	O10-Na1-O9	102.4(1)

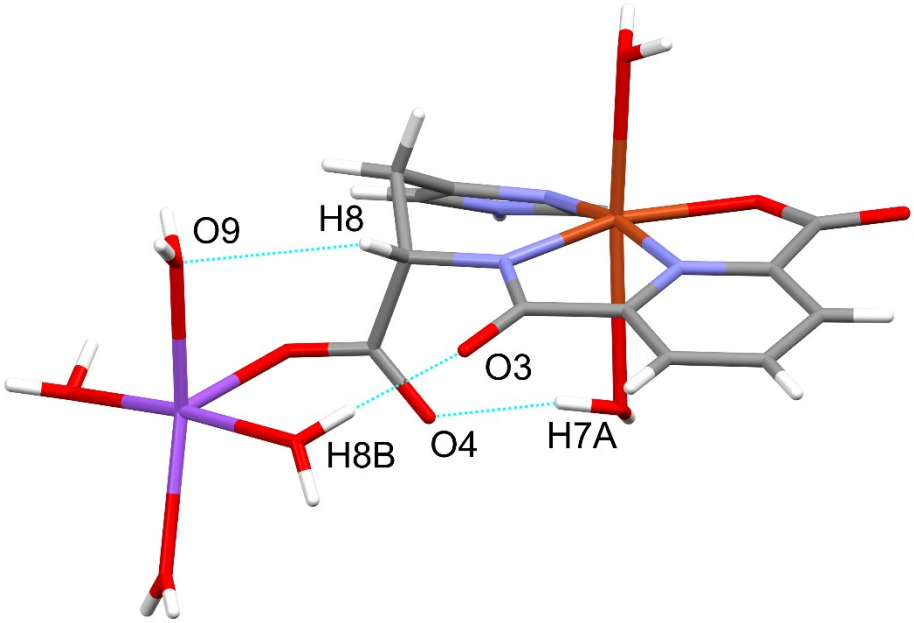

Figure S18. Intramolecular H-bonds in crystal $[Cu(PyHisH_{-1})(H_2O)_2Na(H_2O)_4]$.

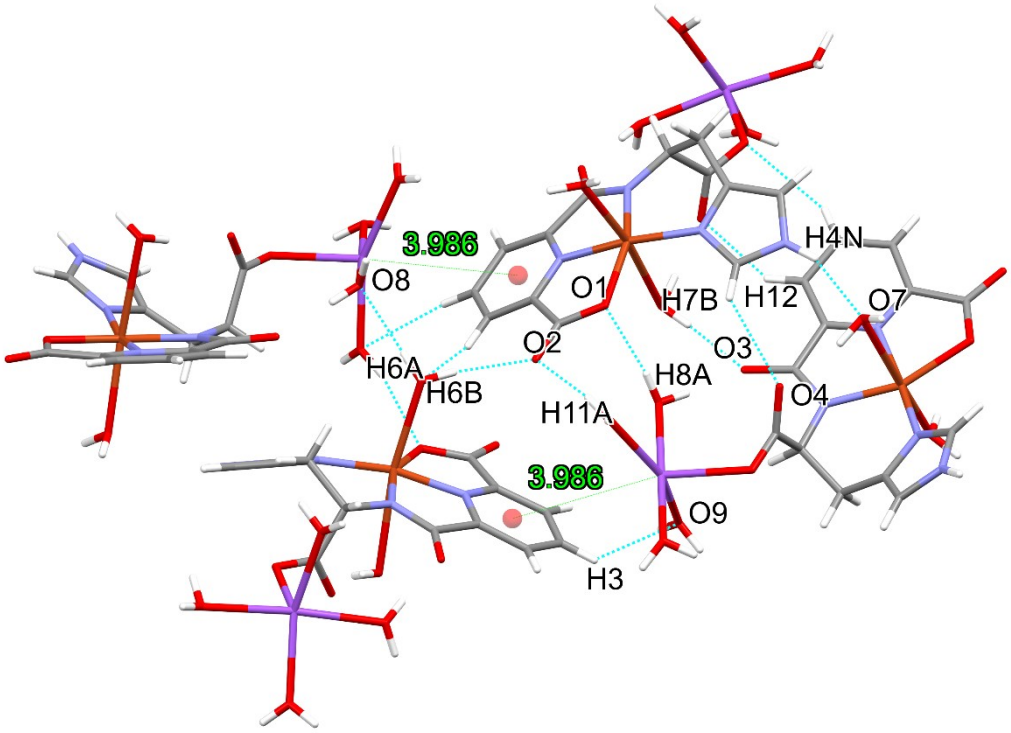

Figure S19. Packing arrangements viewed from the 'cb' plane of crystal $[Cu(PyHisH_{-1})(H_2O)_2Na(H_2O)_4]$ showing the intermolecular H-bond interactions and the distance between pyridine ring centroids and Na^+ ion.

Table S6. Hydrogen-bond geometry of [Cu(PyHisH$_{-1}$)(H$_2$O)$_2$Na(H$_2$O)$_4$].

D-H…A	D-H (Å)	H…A(Å)	D…A(Å)	D-H…A (º)	symmetry codes
N4-H4N…O7	0.88	1.88	2.814(3)	156	1-x,1/2+y,1/2-z
O6-H6A…O8	0.85	2.10	2.942(3)	169	1+x,y,z
O6-H6B…O2	0.85	2.11	2.952(3)	171	1/2+x,1/2-y,1-z
O7-H7A…O4	0.85	1.92	2.758(2)	167	
O7-H7B…O3	0.85	1.93	2.777(3)	176	1-x,1/2+y,1/2-z
O8-H8A…O1	0.85	2.15	2.998(3)	173	
O8-H8B…O3	0.85	1.87	2.717(3)	177	1-x,1/2+y,1/2-z
O9-H9C…O10	0.85	1.96	2.795(3)	169	
O9-H9D…O1	0.85	2.15	2.988(3)	167	1-x,-1/2+y,1/2-z
O10-H10A…O4	0.85	1.87	2.721(3)	173	
O10-H10B…O11	0.85	2.05	2.883(3)	168	
O11-H11A…O2	0.85	2.05	2.871(1)	162	1-x,-1/2+y,1/2-z
O11-H11B…O5	0.85	1.93	2.758(3)	164	-1/2+x,1/2-y,-z
C4-H4…O4	0.85	2.39	3.192(4)	142	1-x,-1/2+y,1/2-z

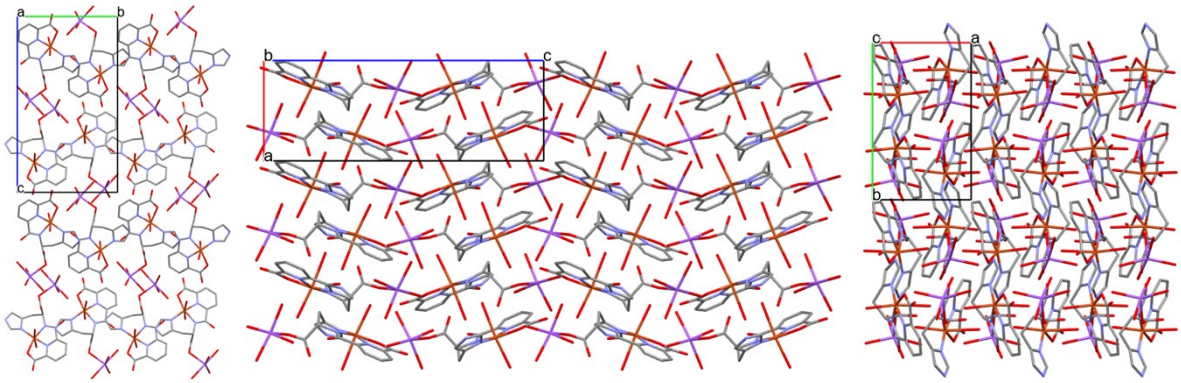

Figure S20. Packing arrangements in crystal [Cu(PyHisH$_{-1}$)(H$_2$O)$_2$Na(H$_2$O)$_4$] viewed from the crystallographic directions ’a’, ’b’ and ’c’.

S6. UV-Vis and CW-EPR spectra of the Cu(II)/PydiHis system

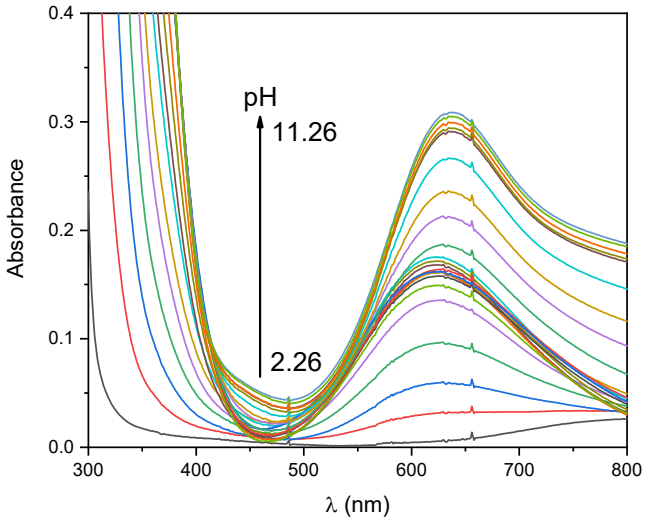

Figure S21. pH-dependent UV-Vis spectra for Cu(II)/PydiHis 1:1 system. c_{Cu} = 1.67 mM.

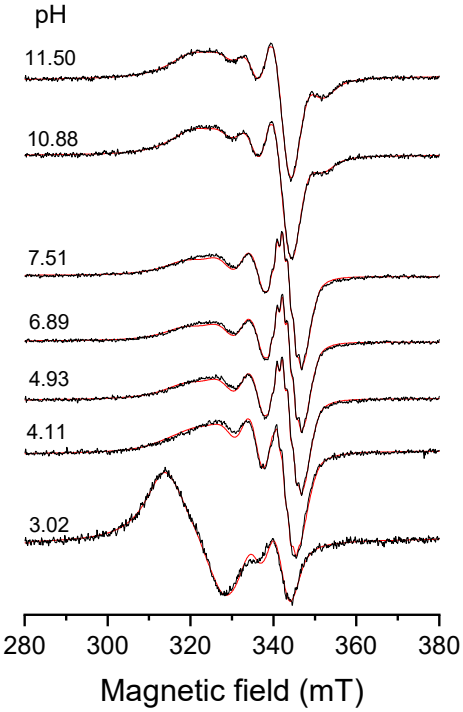

Figure S22. pH dependent experimental (black) and simulated (red) solution EPR spectra recorded in the Cu(II)-PydiHis system at concentration $c_L = c_{Cu}$ = 1.90 mM in aqueous solution at 295 K.

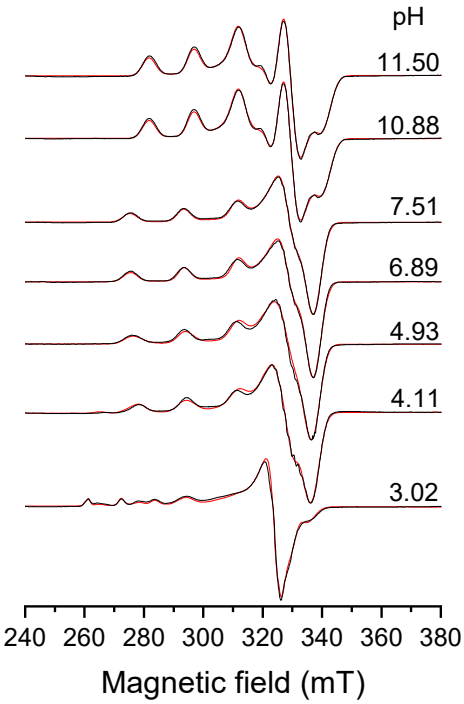

Figure S23. pH dependent experimental (black) and simulated (red) frozen solution EPR spectra recorded in the Cu(II)–PydiHis system at concentration $c_L = c_{Cu} = 1.90$ mM in aqueous solution at 77K.

S7. Superoxide dismutase activity

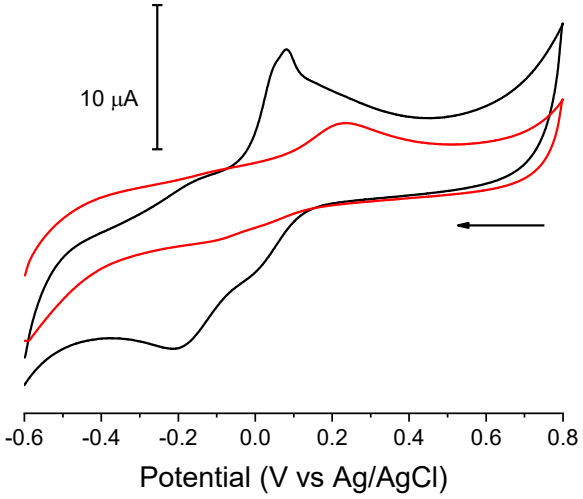

Figure S24. Cyclic voltammograms recorded in the Cu–PyHis (black) and Cu–PydiHis systems at 1:1 metal to ligand concentration ratio and at pH 7.6 (0.2 M KNO_3 supporting electrolyte, glassy carbon electrode, room temperature). The arrow indicates the direction of the scan. $c_{Cu(II)}$ = 2 mM, υ = 200 mVs^{-1}.

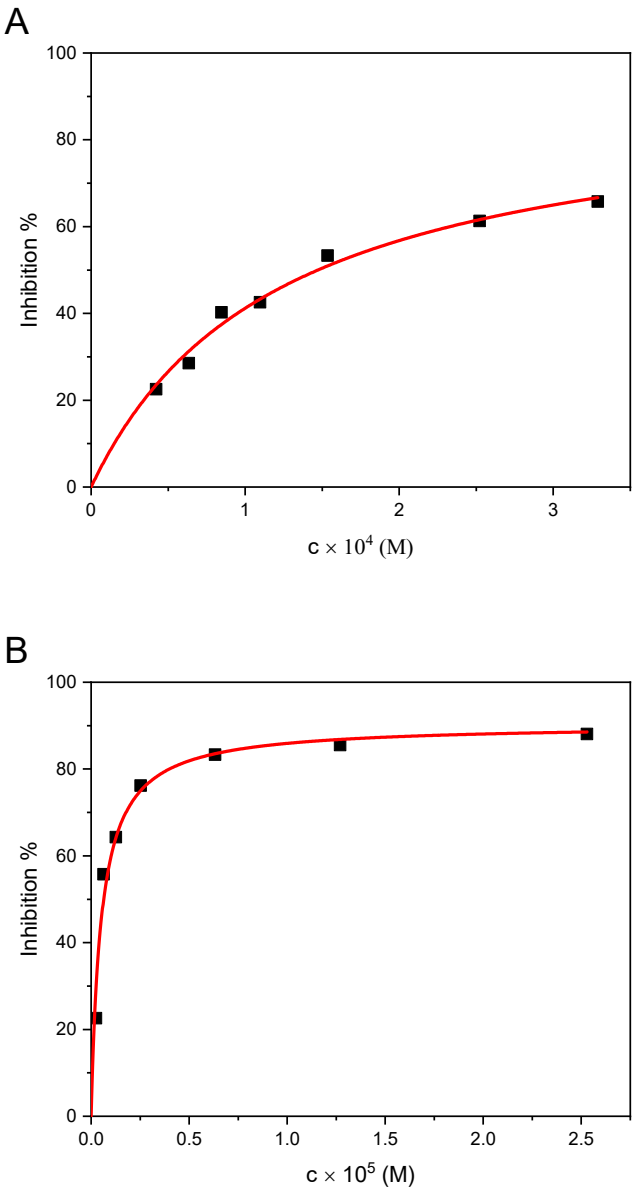

Figure S25. Inhibition percentage as a function of the concentration of the copper(II) complex formed with PyHis (A) and PydiHis (B) at pH 7.6. Inhibition curves were fitted to a saturation curve: $y = P1 \times x/(P2+x)$.

A

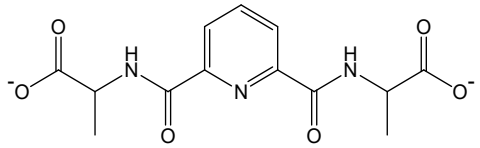

B

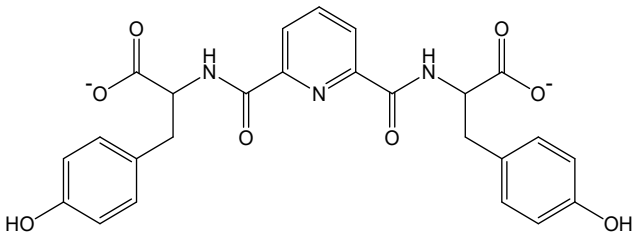

Scheme S2. Structural formulae of the deprotonated form of PydiAla (A) and PydiTyr (B).

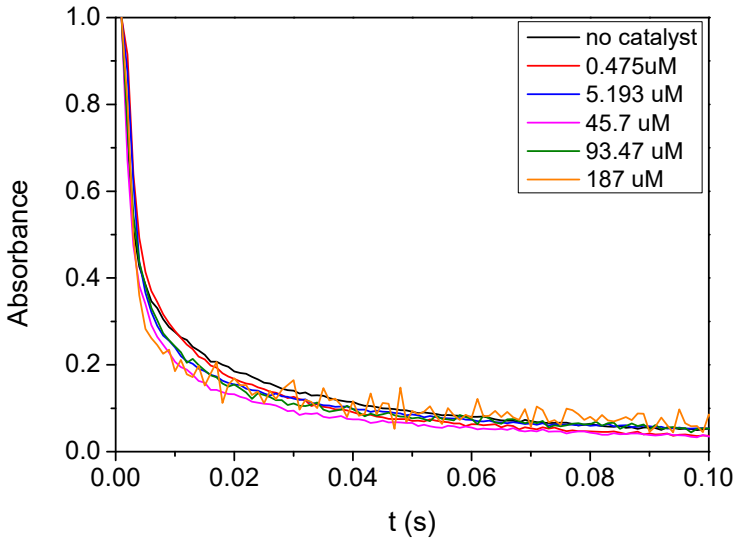

Figure S26. Decomposition of the superoxide anion recorded at 260 nm in the presence of copper(II)-PyHis complex at pH 7.6. The traces were corrected with the absorbance of the complex for better comparison. $c(O_2^{-})^0 = 469$ μM, $\lambda = 260$ nm, $T = 25$ °C, $l = 0.2$ cm.

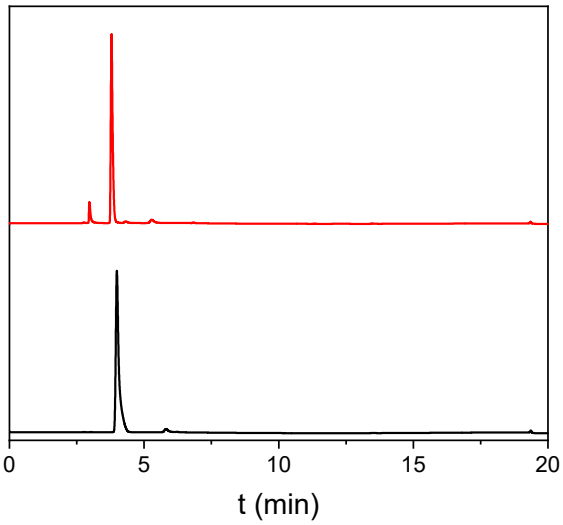

Figure S27. HPLC chromatograms recorded for the $[Cu(PydiHisH_{-1})(H_2O)]^-$ complex before (black) and after the addition of KO_2 (dissolved in DMSO) solution (red).

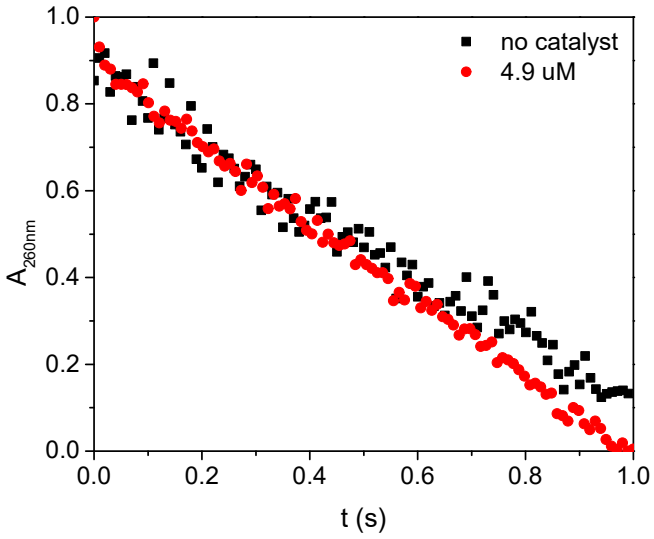

Figure S28. Decomposition of the superoxide anion recorded at 260 nm in the presence of copper(II)-PydiHis complex at pH 9.1. The traces were corrected with the absorbance of the complex for better comparison. $c(O_2^-)^0 = 413$ μM, $\lambda = 260$ nm, $T = 25$ °C, $l = 0.2$ cm.

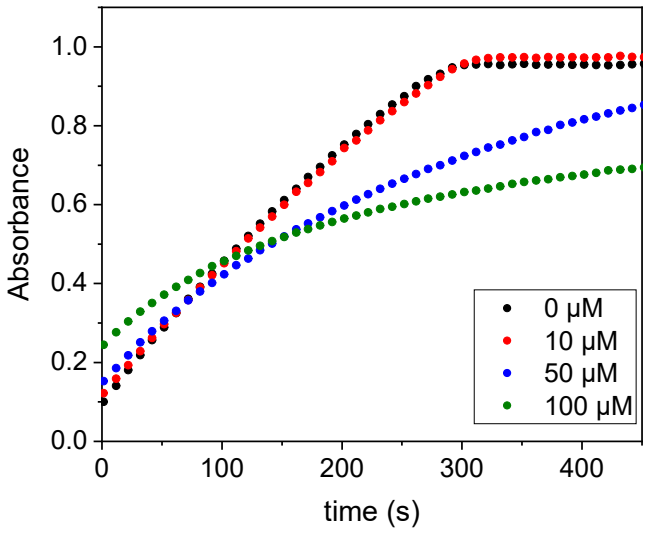

Figure S29. Kinetic traces recorded in the xanthine/xanthine-oxidase system (in the absence of NBT) in the presence of $[Cu(PydiHisH_{-1})(H_2O)]^-$ complex at pH 7.6. The traces were monitored at 300 nm, corresponding to the absorption maximum of uric acid.

S8. DFT and pulsed EPR data

a. DFT results of $[Cu(PyHisH_{-1})H_2O]^-$

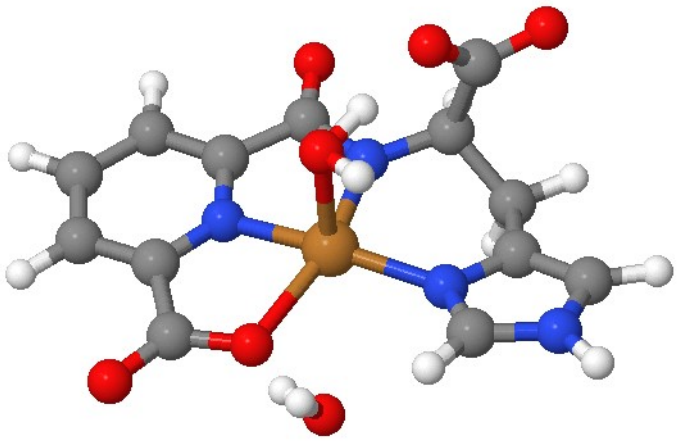

Figure S30. Representation of DFT-optimized structure of $[Cu(PyHisH_{-1})]^-$ in presence of two water molecules. Representation using molviewer option in MatlabR2024a. Several optimization and solvation attempts were performed, resulting all in the formation of square pyramidal structure with the second water no longer coordinating to the copper ion.

Table S7. Cartesian coordinates (in Å) of $[Cu(PydiHisH_{-1})H_2O]^-$ from Figure S30.

Atom	*x*	*y*	*z*
Cu	5.30829762000137	3.91473233140843	6.64608270847312
O	5.60380051644394	0.24242911700092	4.85207005722257
O	3.21068476789436	4.18160454498737	5.76425743040443
H	3.49768594874696	3.80932766585725	4.84624375865231
H	3.15045795818181	5.14139763589236	5.59084683248796
O	5.38944478588393	3.30051021992809	1.72396446426398
O	4.06928018502600	4.13041832813597	10.57446325818026
O	3.87445858961993	3.37008110121589	3.39445336221554
O	4.92089124143270	4.73997604572902	8.56340822836761
O	7.75186496519566	4.38329988130693	8.53197776558675
H	6.81083531224448	4.66449366232704	8.63860012710901
H	7.70485284811085	3.44479593021653	8.80018636683537
N	4.91686392866119	2.30888915121628	7.66545400826968
N	6.03380744915177	5.46137997305262	5.65542150578359
N	6.23685754305719	7.47707626110677	4.79168816242275
H	6.15591254664340	8.49230029677970	4.68283078247762
N	5.80713191044048	2.53568905793523	5.27102726797590
C	5.01757043031332	1.13606339442517	7.01796876864999
C	5.74754515643411	6.75641597885364	5.82935938872602
H	5.19806105534412	7.18881546662783	6.67310249289241
C	5.05276475250555	3.20895974838159	2.92905472724548
C	7.25326550405803	4.03048352645088	3.94072363091723
H	8.12817034216004	3.71756359009504	4.55352127590919
H	7.61295731287941	4.17916329853901	2.90442857087168
C	6.22621436563628	2.86966528636329	3.92895830772089
H	6.73547413728053	1.98779066738265	3.47866646184913
C	4.48783295565392	2.42760111001764	8.92982475924901
C	4.66434578542160	-0.05224668723825	7.67910595345734
H	4.74631243021395	-1.01166670704512	7.14786109939523
C	4.47124364402678	3.87290161506555	9.43160079558112
C	6.72982322241905	5.34182458694307	4.45601603106614
C	6.85677769454351	6.61156342185730	3.91030334631970

H	7.33448317421533	6.96051168379344	2.98937604055995
C	4.11517467536896	1.28179069229891	9.65167431302770
H	3.76254723004211	1.37995188107760	10.68850106327936
C	4.21078356700041	0.03121563590304	9.00987955616772
H	3.92749673235281	-0.88515337707274	9.55060265857048
C	5.50970771539370	1.25461398318369	5.58591467181526

Table S8. Computed principal *g*, copper hyperfine (^{Cu}A) and selected proton hyperfine values of the DFT-optimized $[Cu(PyHisH_{-1})(H_2O)]^-$ complex.

	x	*y*	*z*	α,β,γ /°
g	2.0435	2.0529	2.1507	0,0,0
^{Cu}A /MHz	59.8	13.2	-549.9	33,1,-31
^{Ha}A /MHz	18.4	22.5	17.5	-160,22,150
^{H1}A (H_2O)/MHz	-3.6	-3.1	6.7	-54,20,67
^{H2}A (H_2O) /MHz	-3.1	-3.1	5.5	-20, 21,24

Table S9. Computed principal hyperfine (*A*) and nuclear quadrupole (*P*) values of the ^{14}N nuclei of the DFT-optimized $[Cu(PyHisH_{-1})(H_2O)]^-$ complex.

Nucleus	A_x /MHz	A_y /MHz	A_z /MHz	α,β,γ /°	P_x /MHz	P_y /MHz	P_z /MHz	α,β,γ /°
His N_ε	2.08	1.64	1.41	-138, 17,149	-0.52	-0.74	1.26	-147,15,113
His N_δ	35.69	27.46	28.03	-91,18,97	-1.06	1.02	0.04	-111,15,119
Pyridine N	55.71	42.00	43.13	145,4,-145	-1.58	0.81	0.77	-122,2,122
Amide N	39.87	59.57	41.72	-158,6,173	1.36	-0.43	-0.93	165,3,-152

b. HYSCORE results of $[Cu(PyHisH_{-1})H_2O]^-$

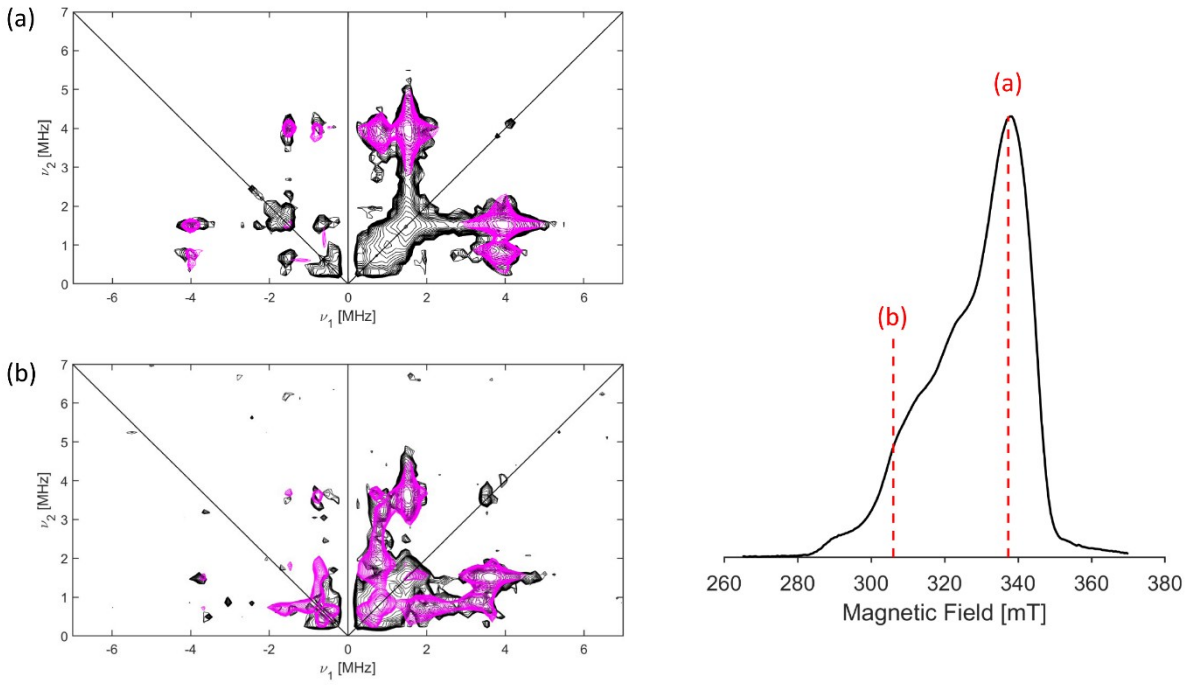

Figure S31. (Left) ^{14}N-HYSCORE spectra of a frozen solution of Cu(II)-PyHis at pH 7.0 (1:1 Cu:L) at field positions (a) 337.7 mT and (b) 306.0 mT. The experimental τ-value was 120 ns. These observer positions are indicated in the ESE-detected EPR spectrum (right). Black: experiment, magenta: simulations using the hyperfine and quadrupole values of the remote N_ε of the imidazole residue of His in Table S10.

Table S10. Principal hyperfine (A) and nuclear quadrupole (P) values of selected ^{1}H and ^{14}N nuclei of the $[Cu(PyHisH_{-1})]^-$ complex as used for the simulations of the pulsed EPR experiments in Figure S31, S33 and Figure 6a. The Euler angles were taken from the DFT computations (Tables S8-S9). H_a indicates the proton of the α carbon of the His fragment.

Nucleus	A_x/MHz	A_y/MHz	A_z/MHz	α,β,γ /°	P_x/MHz	P_y/MHz	P_z/MHz	α,β,γ /°
His N_ε	1.50	1.75	1.10	-138,17,149	-0.69	-0.08	0.77	-147,15,113
H_a	9.0	13.5	9.0	-160,22,150	-	-	-	-

c. HYSCORE results of $[Cu(PydiHisH_{-1})H_2O]^-$

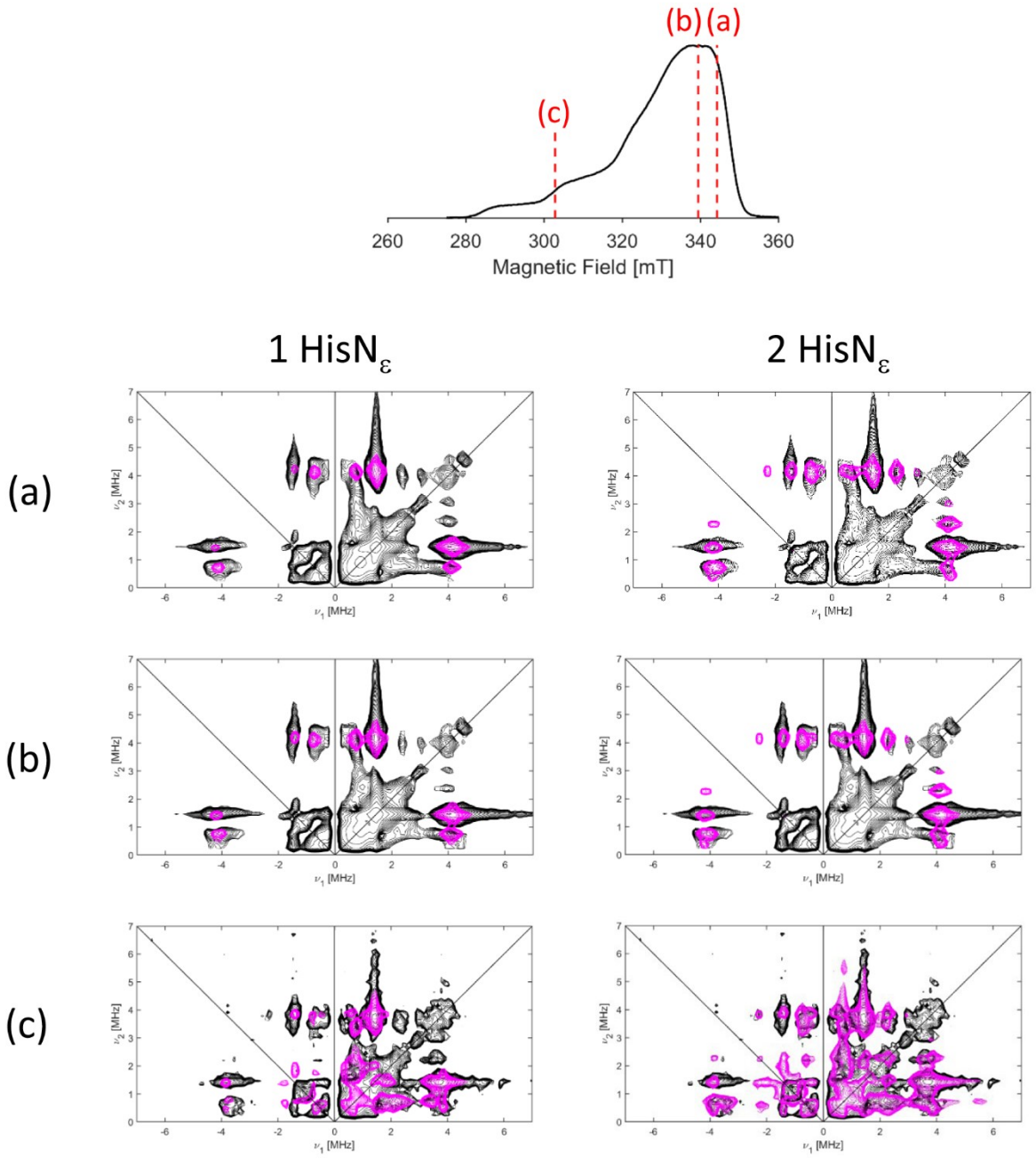

Figure S32. (Top) ESE-detected EPR spectrum of a frozen solution of Cu(II)-PydiHis at pH 7.0 (1:1 Cu:L). **(below)** ^{14}N-HYSCORE spectra corresponding to the field positions (a) 344.2 mT, (b) 339.4 mT and (c) 302.8 mT as indicated in the top ESE-detected EPR spectrum. The experimental τ-value was 120 ns. Black: experiment, magenta: simulations using the hyperfine and quadrupole values of the remote N_ε of the imidazole residue of His in Table S11. **Left**: considering only the contribution of one ^{14}N, **right**: considering the contribution of both ^{14}N nuclei.

Table S11. Principal hyperfine (A) and nuclear quadrupole (P) values of selected ^{1}H and ^{14}N nuclei of the $[Cu(PydiHisH_{-1})]^{-}$ complex as used for the simulations of the pulsed EPR experiments in Figures S32, S34 and Figure 6b. H_a indicates the proton of the α carbon of the His fragment. H_w indicates protons of the copper-coordinated water molecule, remote H indicates a proton from the surrounding water matrix.

Nucleus	A_x/MHz	A_y/MHz	A_z/MHz	α,β,γ /°	P_x/MHz	P_y/MHz	P_z/MHz	α,β,γ /°
His $^{1}N_{\varepsilon}$	1.80	2.00	1.30	-138, 17,149	-0.66	-0.08	0.74	-147,15,113
His $^{2}N_{\varepsilon}$	2.00	1.80	1.30	-138, 17,149	-0.08	-0.66	0.74	-147,15,113
H_a	7.0	11.0	5.5	-160,20,120	-	-	-	-
H_w H_2O	-2.8	-2.8	6.7	-54,32,67	-	-	-	-
Remote H	-0.1	-0.1	0.2	0,0,0	-	-	-	-

d. ENDOR experiments of $[Cu(PyHisH_{-1})H_2O]^{-}$ and $[Cu(PydiHisH_{-1})H_2O]^{-}$

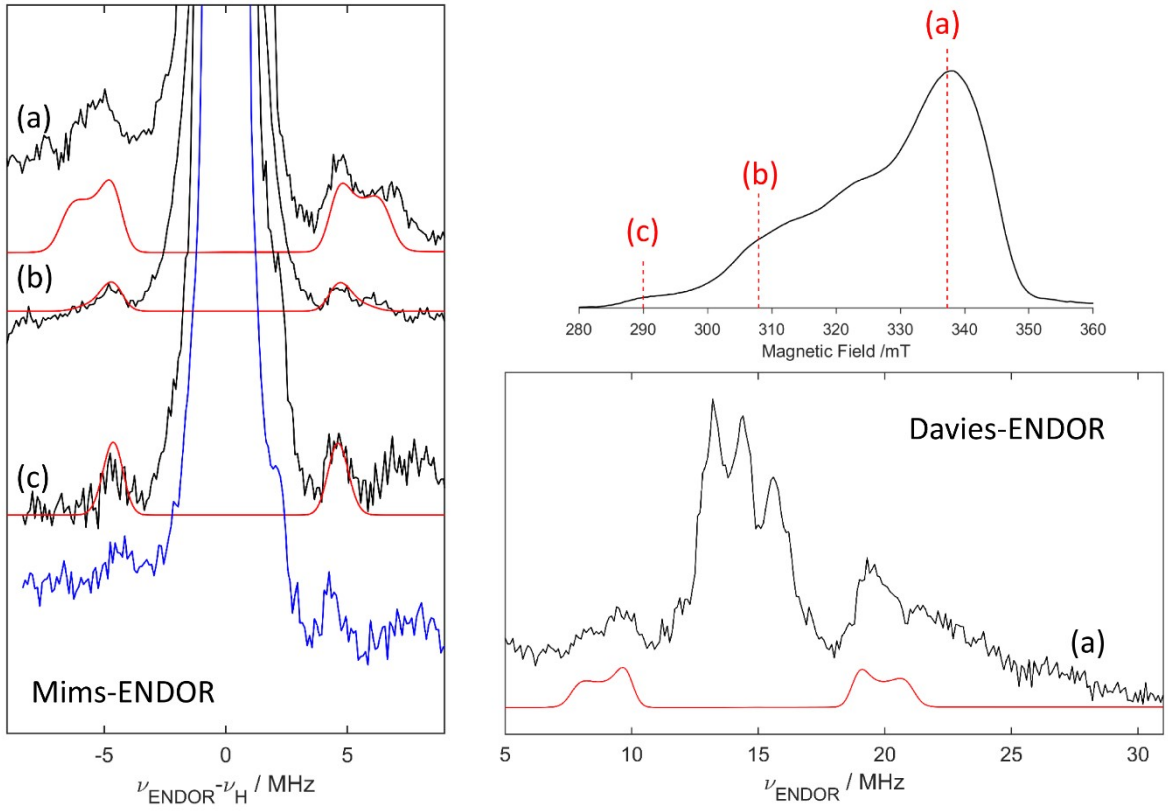

Figure S33. (Left) ^{1}H-Mims ENDOR spectra of a frozen solution of Cu(II)-PyHis at pH 7.0 (1:1 Cu:L) at field positions (a) 337.7 mT, (b) 308.0 mT and (c) 290.0 mT. The spectra are shown centred around the proton Larmor frequency (ν_H). The Mims-ENDOR spectra are the sum of experimental τ-values ranging from 104 ns to 168 ns in steps of 16 ns.
(Right, bottom) Davies ENDOR spectrum of the same sample at observer field (a) 337.7 mT. The observer positions are indicated in the ESE-detected EPR spectrum **(Right, top)**.
Black: experiment for complex in H_2O, blue: experiment for complex in D_2O, red: simulations using the hyperfine values of H_a in Table S10.

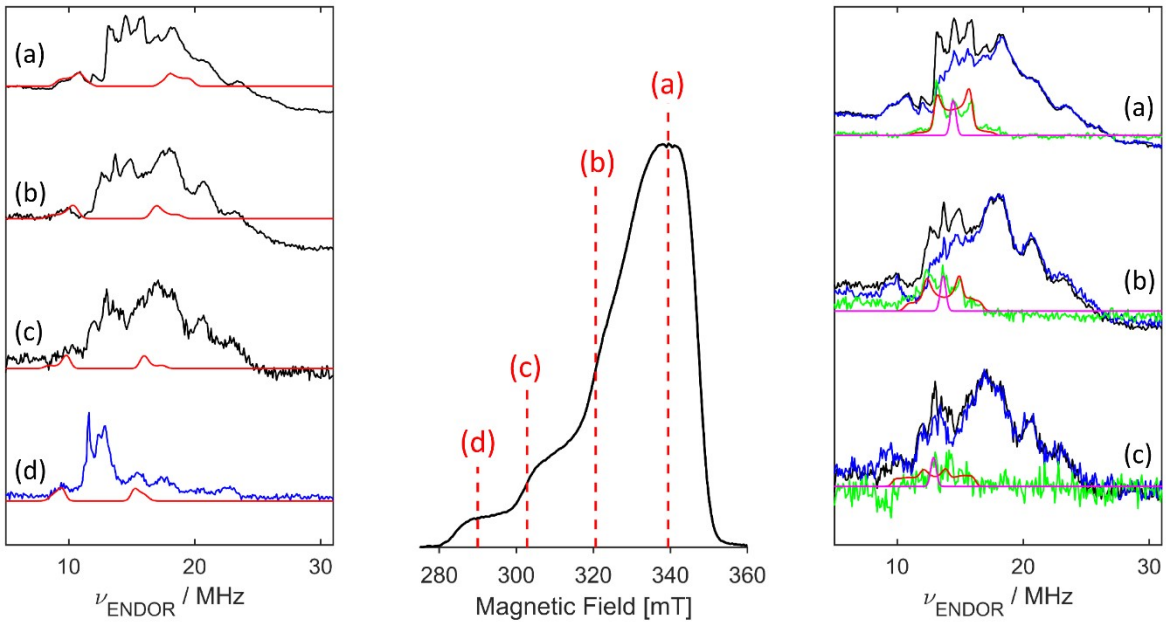

Figure S34. **(left, right)** ENDOR experiments of a frozen solution of Cu(II)-PydiHis at pH 7.0 (1:1 Cu:L) at observer positions (b) 339.4 mT, (b) 320.6 mT, (c) 302.8 mT and (d) 290.0 mT as indicated in the ESE-detected EPR spectrum **(middle)**.
Black: experiments in H_2O, blue: experiments in D_2O.
Left (a,b,c) Davies ENDOR, (d) Mims-ENDOR with τ = 104 ns. Red: simulations using the hyperfine values of H_a in Table S11.
Right. Davies-ENDOR spectra. Green: subtraction between the spectra of the complex in H_2O and D_2O representing the ENDOR spectrum of the exchangeable protons. Red: simulations using the hyperfine values of H_w (protons of copper-coordinated water) in Table S11, magenta: simulations using the hyperfine values of a remote proton in Table S11.

e. DFT, HYSCORE and ENDOR of $[Cu(PydiHisH_{-2})]^{2-}$

The *g* and copper hyperfine values of a frozen solution of Cu(II)-PydiHis at pH 12.0 strongly deviate from those at pH 7.0 (Table S2, Figure 3(right,top), Figure S37). Indeed, DFT calculation predicts a significant change in these parameters for the $[Cu(PydiHisH_{-2})]^{2-}$ complex (Table S12) as compared to $[Cu(PyHisH_{-1})H_2O]^{-}(H_2O)$ (Table S8). Interestingly, the DFT-computed structure of $[Cu(PydiHisH_{-2})]^{2-}$ reveals N_{py}-Cu-N_{His} and $N_{carboxamide}$-Cu-$N_{carboxamide}$ angles of 121.5° and 160.9° (Table S13), close to the ones predicted in the main text on the basis of the experimental copper A_z value (Figure S35, Table S12).

The HYSCORE spectra of a frozen solution of Cu(II)-PydiHis at pH 12.0 unusually feature numerous low intensity cross peaks. Figure S36a shows an example of such a HYSCORE spectrum. Next to the low-frequency region where the cross-peaks due to the His N_ε nitrogen(s) are expected (marked in green) and the ^1H region (marked in magenta), extended ridges are observed in the (-,+) quadrant (signals marked in blue). The ridges are separated by 4× the Larmor frequency of ^{14}N (ν_N), identifying them as double-quantum ridges of strongly coupled ^{14}N nuclei. These signals match the broad lines observed in the Davies-ENDOR and Mims-ENDOR spectra below 10 MHz (indicated by the same color code in the exemplary Davies-ENDOR spectrum in Figure S36b). The ENDOR spectra contain also contributions of ^1H hyperfine interactions as well as signals in the region of 15-35 MHz that can be ascribed to strongly coupled ^{14}N nuclei. Note that the contributions of the strongly coupled ^{14}N nuclei are still clearly visible in the Mims ENDOR spectra (Figure S37), which is quite unusual.

The ^{14}N HYSCORE spectra of the frozen solution of Cu(II)-PydiHis at pH 12.0 reveal a pattern of cross-peaks in the low-frequency area (His N_ε contribution) that only marginally change with magnetic field (Figure S36c, Figure S38) and that strongly differ from those observed at pH 7.0 (Figure S32). The latter difference is due to a decrease in the hyperfine values of the His N_ε for the pH 12.0 case (compare Table S10 and Table S11). Unfortunately, the spectral simulations do not allow us to determine whether one or two His residues bind to the metal ion (Figure

S38). To our knowledge, the lowered HisN_ε hyperfine values have only been reported once, namely for a Cu(II) complex of the His brace in lytic polysaccharide monooxygenase at high pH.[4] In that specific case, the reduction of the hyperfine interaction was ascribed to the deprotonation of the His N_ε at pH 12.5. The pK_a of the transition between the neutral imidazole and imidazolate anion of His is 14.5, however the presence of copper(II) may induce this deprotonation and decrease the pK_a by about three orders of magnitude compared to the free ligand.[5] This effect is found to be more pronounced, when copper(II) is applied in excess, and the His N_ε provides an additional binding site for copper(II). The decrease of the His N_ε hyperfine values could also be related to the changes in the electronic ground state. In fact, DFT calculations predict a reduction of the His N_ε hyperfine coupling alongside with a significant decrease in the His N_δ hyperfine values when $[Cu(PyHisH_{-1})H_2O]^-(H_2O)$ (Table S9) and $[Cu(PydiHisH_{-2})]^{2-}$ (Table S15) are compared. It is unclear whether the trends of the His N_ε and His N_δ hyperfine couplings are linked, since a combined HYSCORE and ENDOR study of Cu(II) complexes of cupredoxin azurin variants found no direct correlation between these couplings, with the His N_ε hyperfine values being always in the same range as found here for the complexes formed at pH 7.0.[6]

In order to disentangle the ^{14}N ENDOR features form the ^{1}H features, a simultaneous ^{1}H HYSCORE and ^{1}H Mims-ENDOR simulation of the contributions of the most strongly coupled protons was performed (Figure S39, Table S14). Comparison with the DFT model predicts these to be the protons of the α-carbon of His (Table S12). All other DFT-computed proton couplings are smaller than 4 MHz, as is also observed experimentally.

The Davies-ENDOR peaks in the 15-35 MHz range can be simulated assuming the contribution of three ^{14}N nuclei with principal hyperfine values ranging from 35 to 55 MHz (Table S14, Figure S40). Furthermore, the broad signals in the 1-14 MHz range in the ENDOR spectra (Figure S40) and in the (-,+) quadrant of the HYSCORE spectra (Figure S39) indicate the

contributions of ^{14}N nuclei with considerably lower hyperfine values (in the order of 5-20 MHz). The ENDOR spectra do not reveal any substructure in this region and also the HYSCORE spectra show extended ridges, indicating considerable hyperfine and quadrupole strain, which in turn points to conformational flexibility.[7] The ENDOR and HYSCORE spectra cannot perfectly be simulated due to the lack of resolution, but a simulation using hyperfine values spreading from 6-16 MHz show reasonable agreement (Figure S40, Table S14). These values are in qualitative agreement with the DFT model, predicting considerably stronger hyperfine couplings for the directly coordinated nitrogen atoms of pyridine and of the amides than for the His N_δ nuclei (Table S14). Moreover, the imidazole rings of the histidines are expected to exhibit considerably more conformational flexibility than the pyridine and amide part, explaining the featureless ENDOR lines for the His N_δ nuclei.

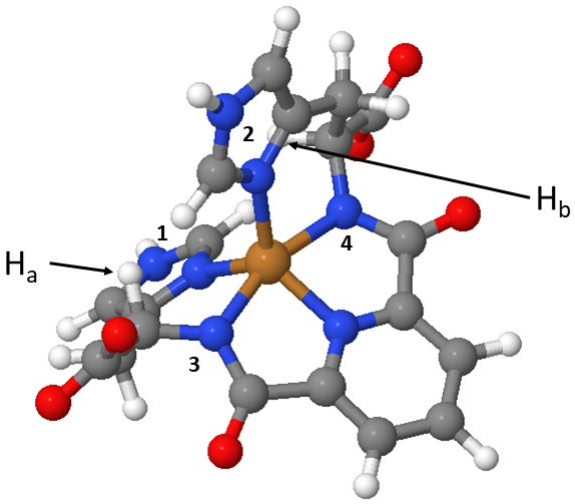

Figure S35. Representation of DFT-optimized structure of $[Cu(PydiHisH_{-2})]^{2-}$. Representation using molviewer option in MatlabR2024a. The protons H_a and H_b on the α-carbons are indicated.

Table S12. Computed principal ***g*** and copper hyperfine (^{Cu}A) values of the DFT-optimized $[Cu(PydiHisH_{-2})]^{2-}$ complex. The g_y axis is pointing along the Cu-N_{py} axis, while the g_x axis is

more or less along the $N_{carboxamide}$-Cu-$N_{carboxamide}$ axis. Also the ^1H hyperfine coupling of protons H_a and H_b is given. All other ^1H hyperfine couplings had maximum values below 4 MHz.

	x	*y*	*z*	α,β,γ /°
g	2.0086	2.0965	2.1319	0,0,0
^{Cu}A /MHz	255.4	-152.0	-367.3	-1,1,1
^{Ha}A /MHz	7.05	14.63	6.19	-113,2,69
^{Hb}A /MHz	7.05	14.63	6.19	113,2,-69

Table S13. Cartesian coordinates (in Å) of $[Cu(PydiHisH_{-2})]^{2-}$ depicted in Figure S37.

Atom	*x*	*y*	*z*
C	1.18174778577224	2.49384102318914	0.14093339624307
C	-1.18219858768037	2.49367558605480	-0.13880125891239
C	-1.21956682419774	3.89990944157179	-0.13886187059512
C	-0.00046061875855	4.59628309242614	0.00180472385791
C	1.21880123952626	3.90008469225772	0.14197498489895
H	-2.17982793145880	4.42576942346820	-0.24554240421008
H	-0.00058362180241	5.69776327380369	0.00220441781313
H	2.17893725094651	4.42609475123639	0.24904249919876
N	-0.00015366148121	1.87471720855224	0.00083784043962
C	-2.37112245534987	1.53234052920476	-0.20906951074975
C	2.37086471084282	1.53270247030767	0.21047938237983
O	-3.54598854873486	1.97428445390159	-0.13852466061535
O	3.54562276559300	1.97493703540948	0.13982749011450
N	-1.95322966568992	0.25183422100050	-0.31291374890832
C	-2.83946942072096	-0.88240332157226	-0.09248796013066
H	-2.28486228828431	-1.77414050394144	-0.46812732225798
C	-3.05789980395089	-1.10073462149351	1.41819793111424
C	-4.14960650682369	-0.88083873513464	-0.97566187595612
H	-3.49164346831799	-0.16785590334174	1.84386214431862
H	-3.83168501617396	-1.88137767593179	1.56467554951882
C	-1.80037158775570	-1.48104653031630	2.16746764976102
O	-5.25693169859197	-1.04452075459773	-0.39338486261897
N	-0.51371947121875	-1.16754694544718	1.73293073848319
C	-1.69164866867359	-2.14275738151702	3.38604990681993
C	0.33971680478576	-1.60656796918458	2.66359739907545
N	-0.34120034477884	-2.20373901593853	3.67647742619718
H	-2.44912760016535	-2.56045438042270	4.05738429158203
H	1.43323400880684	-1.47956671433255	2.64065482158312
H	0.07670347852883	-2.62693928099069	4.50956463415696
O	-3.94087063383492	-0.78104481870903	-2.22266917441902
Cu	0.00002781930237	-0.08027289503438	0.00035333736291
N	1.95332140881546	0.25202240221651	0.31359207105273
C	2.83986209751204	-0.88169967980516	0.09162832753273
H	2.28552933834576	-1.77404256071879	0.46622165017918
C	3.05825467856823	-1.09808224901258	-1.41933964399036
C	4.15012531965649	-0.88079354434571	0.97461158020156
H	3.49181263262994	-0.16456896456501	-1.84380275631408
H	3.83219094546002	-1.87837880651469	-1.56685352721041
C	1.80079384597169	-1.47770683291757	-2.16904691513666
O	3.94151070380401	-0.78298913371384	2.22179995981154
N	0.51411139370547	-1.16522267262620	-1.73393275749354
C	1.69216978405364	-2.13766362188196	-3.38859173759357
C	-0.33931058127780	-1.60347812787259	-2.66496334199812
N	0.34168353307601	-2.19893160311051	-3.67881201857505
H	2.44971590009621	-2.55409717748742	-4.06063543601774

H	-1.43289720251602	-1.47709853777148	-2.64160049487111
H	-0.07618592217025	-2.62123011040282	-4.51237375325611
O	5.25744768460911	-1.04303753394823	0.39193087813360

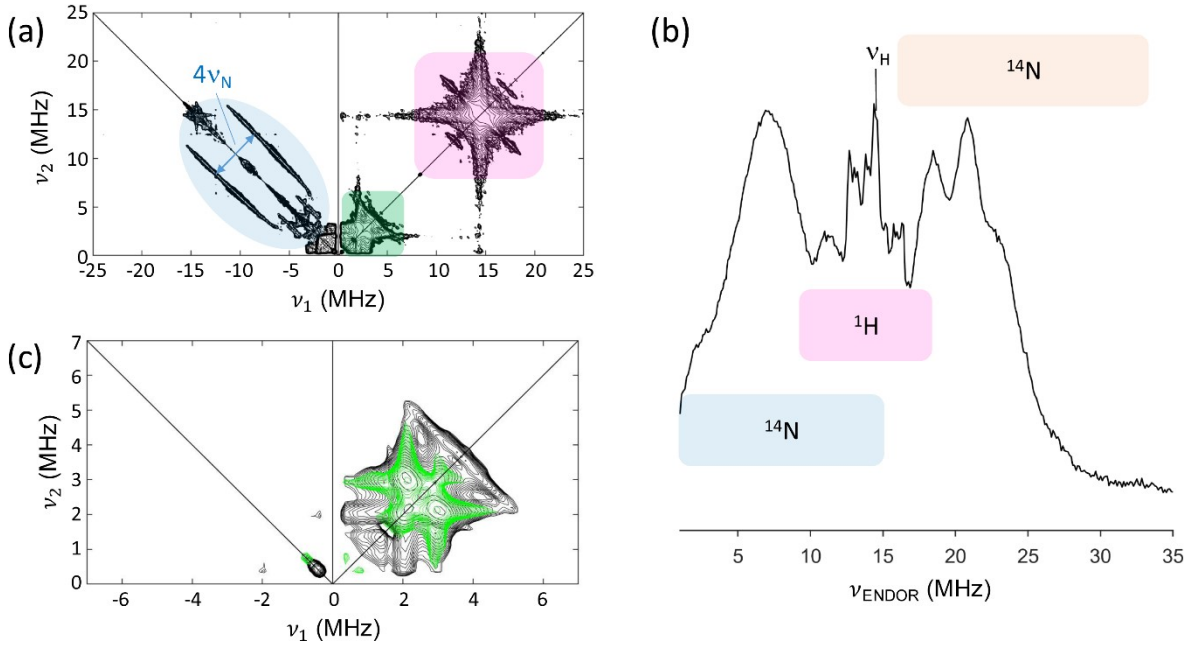

Figure S36. (a) Experimental HYSCORE spectrum of a frozen solution of Cu(II)-PydiHis at pH 12.0 at observer position 339.2 mT. The spectrum is the sum of τ-values 104, 120 and 176 ns. Three regions can be distinguished stemming from protons (magenta), weakly coupled ^{14}N nuclei (green) and strongly coupled ^{14}N nuclei (blue). (b) Example of Davies-ENDOR spectrum of a frozen solution of Cu(II)-PydiHis at pH 12.0 (observer position 325.6 mT). The colour code is similar as in Figure 6a. Orange indicates the contributions of the most strongly coupled ^{14}N nuclei, not observed in the HYSCORE spectra. (c) Low-frequency area of HYSCORE spectrum in (a). The contour lines are set such as to show the strongest peaks in this region. (black) Experiment, (green) simulation using the simulation parameters mentioned in Table S14.

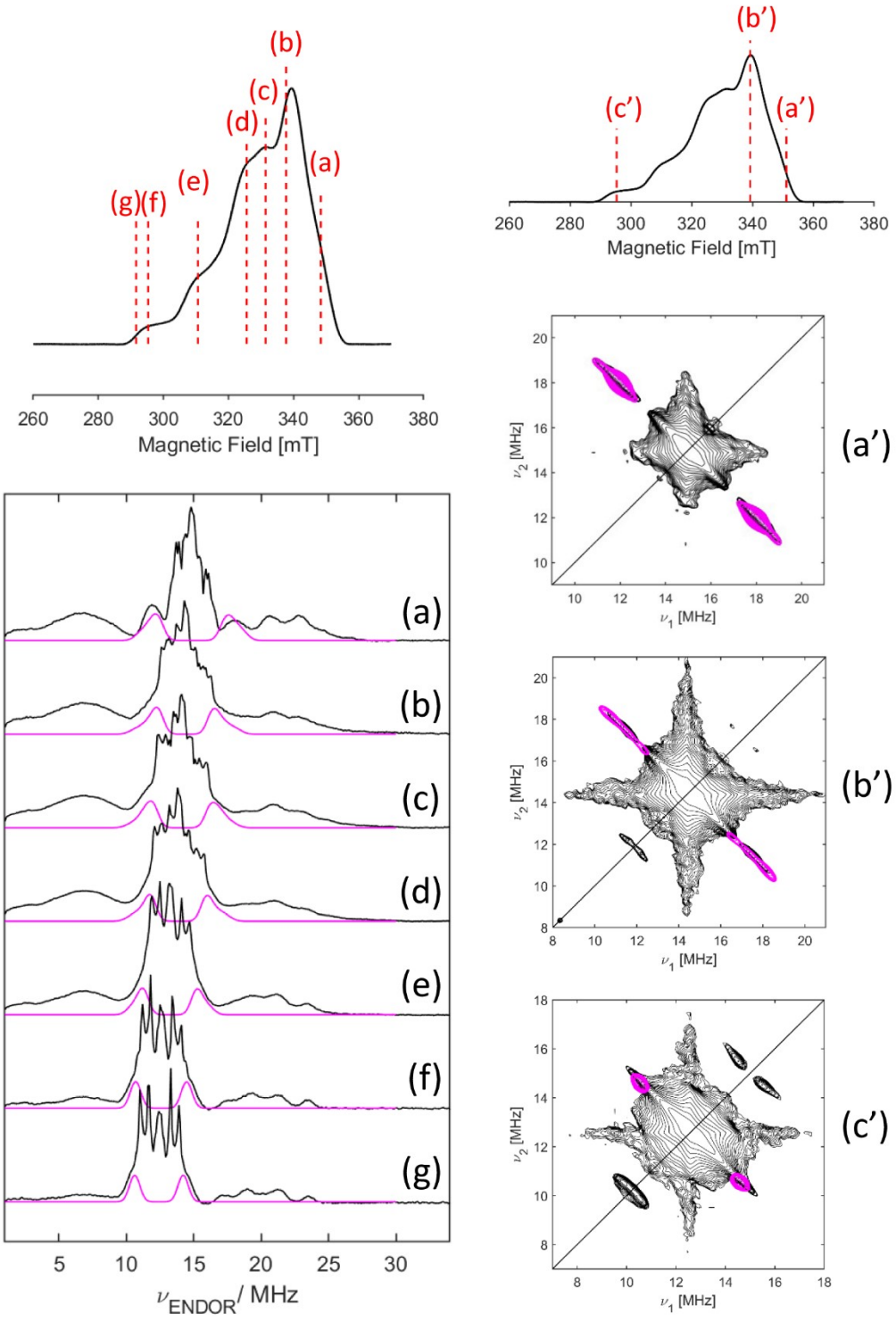

Figure S37. (left) Experimental (black) and simulated (magenta) Mims ENDOR spectra of a frozen solution of Cu(II)-PydiHis at pH 12.0 (1:1 Cu:L). Observer positions are: (a) 348.4 mT, (b) 337.7 mT, (c) 331.4 mT, (d) 325.6 mT, (e) 310.6 mT, (f) 295.3 mT, (g) 291.6 mT as indicated in the ESE-detected EPR spectrum (top).
Right: Experimental (black) and simulated (magenta) ^{1}H HYSCORE spectra of a frozen solution of Cu(II)-PydiHis at pH 12.0 (1:1 Cu:L). Observer positions are: (a') 351.1 mT, (b') 339.2 mT and (c') 295.3 mT as indicated in the top ESE-detected EPR spectrum. All

simulations include only the contribution of protons H_a and H_b with parameters given in Table S14.

Table S14. Principal hyperfine (*A*) and nuclear quadrupole (*P*) values of selected ^{1}H and ^{14}N nuclei of the $[Cu(PydiHisH_{-2})]^{2-}$ complex used for the simulations of the pulsed EPR experiments shown in Figures S36-S40. H_a and H_b are the protons of the α carbons of the His fragments. For the optimization of the simulations, (starting) Euler angles were taken from initial (suboptimal) DFT results and further optimized to match the spectral features.

Nucleus	A_x/MHz	A_y/MHz	A_z/MHz	α,β,γ /°	P_x/MHz	P_y/MHz	P_z/MHz	α,β,γ /°
His(1) N_ε	0.35	0.45	0.7	1,39,-86	0.52	-0.91	0.39	44,61,-19
His(2) N_ε	0.35	0.45	0.7	-1,39,86	0.52	-0.91	0.39	-44,61,19
His(1) N_δ	6	16	8	-3,32,-78	0.55	0.94	-1.49	-4, 48, -78
His(2) N_δ	6	16	8	3,32,78	0.55	0.94	-1.49	4, 48, 78
Pyridine N	42.5	55	35	0,83,0	1.00	-1.52	0.52	0,90,0
Amide(3) N	38	36	48	9,86,-15	-0.68	1.15	-0.47	2,89,-14
Amide(4) N	38	36	48	-9,86,15	-0.68	1.15	-0.47	-2,89,14
H_a	8.5	4.0	3.5	-69,9,102	-	-	-	-
H_b	8.5	4.0	3.5	69,9,-102	-	-	-	-

Table S15. Computed principal hyperfine (*A*) and nuclear quadrupole (*P*) values of the ^{14}N nuclei of the DFT-optimized $[Cu(PydiHisH_{-2})]^{2-}$ complex. Euler angles are versus the ***g*** tensor. The numbering of the His and amide groups are indicated in Figure S35. Visual comparison of the principal orientations of the tensors showed a reasonable fit with those used for the simulations (Table S12).

Nucleus	A_x /MHz	A_y/MHz	A_z/MHz	α,β,γ /°	P_x/MHz	P_y/MHz	P_z/MHz	α,β,γ /°
His(1) N_ε	0.67	0.57	0.95	-95,29,93	0.73	-1.30	0.57	-136,43,143
His(1) N_δ	14.85	15.12	19.19	-86,34,82	1.04	0.29	-1.33	-85,30,82
His(2) N_ε	0.67	0.57	0.95	95,28,-94	0.73	-1.30	0.57	136,43,-143
His(2) N_δ	14.83	15.09	19.16	86,34,-82	1.04	0.29	-1.33	85,30,-82
Pyridine N	43.39	56.18	44.40	-180,6,180	0.86	-1.78	0.91	-180,25,180
Amide(3) N	50.91	33.88	35.45	115,8,-127	-0.66	1.49	-0.83	154,12,-165
Amide(4) N	50.90	33.87	35.44	-114,8,126	-0.66	1.49	-0.83	-154,12,165

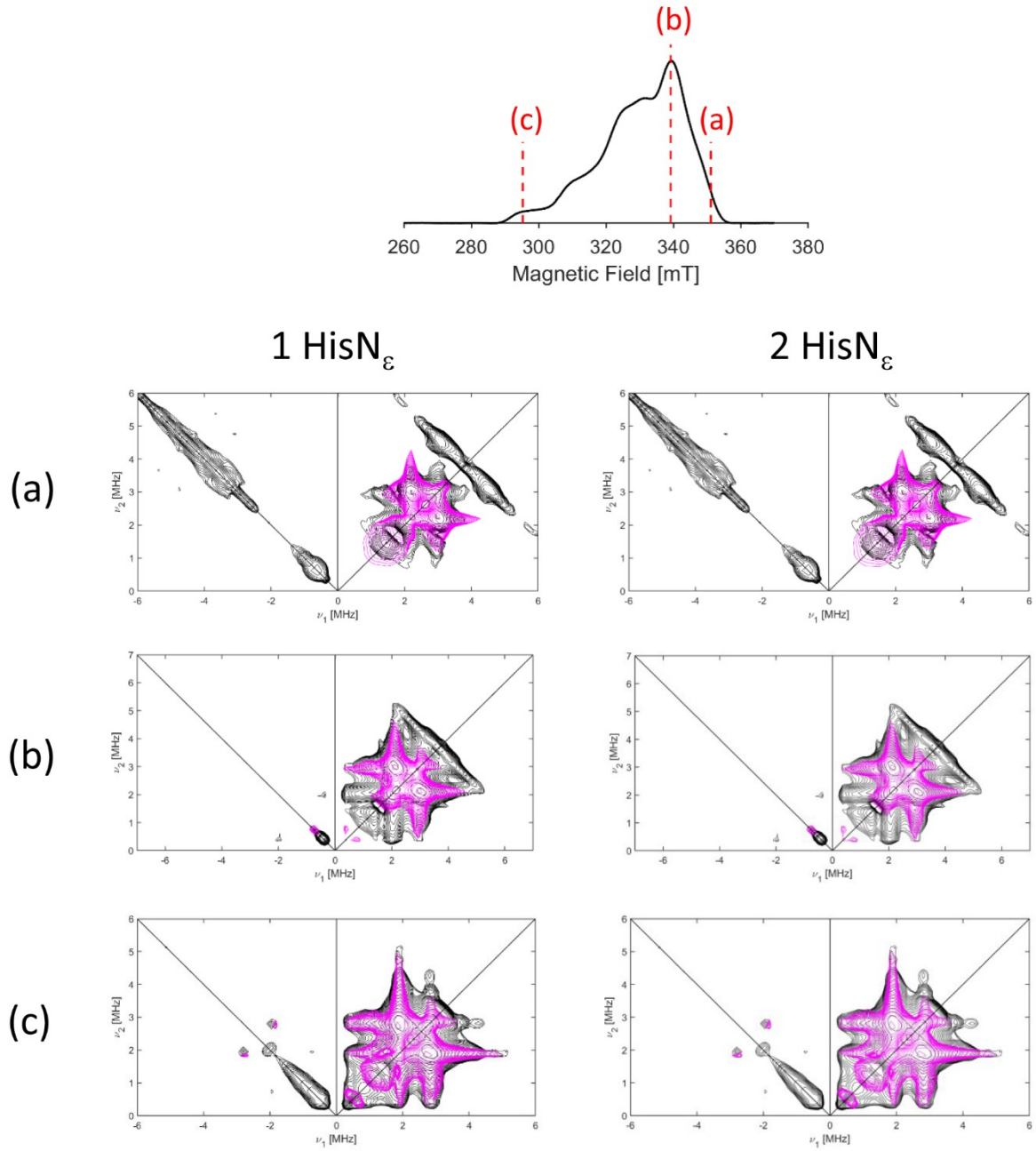

Figure S38. (Top) ESE-detected EPR spectrum of a frozen solution of Cu(II)-PydiHis at pH 12 (1:1 Cu:L). **(below)** ^{14}N-HYSCORE spectra corresponding to the field positions (a) 351.1 mT, (b) 339.2 mT and (c) 295.3 mT as indicated in the top ESE-detected EPR spectrum. The experimental spectra are the sum of τ-values 104, 120 and 176 ns. Black: experiment, magenta: simulations using the values of the remote N_ε of the imidazole residue of His in Table S14. Left: considering only the contribution of one ^{14}N, right: considering the contribution of two ^{14}N nuclei.

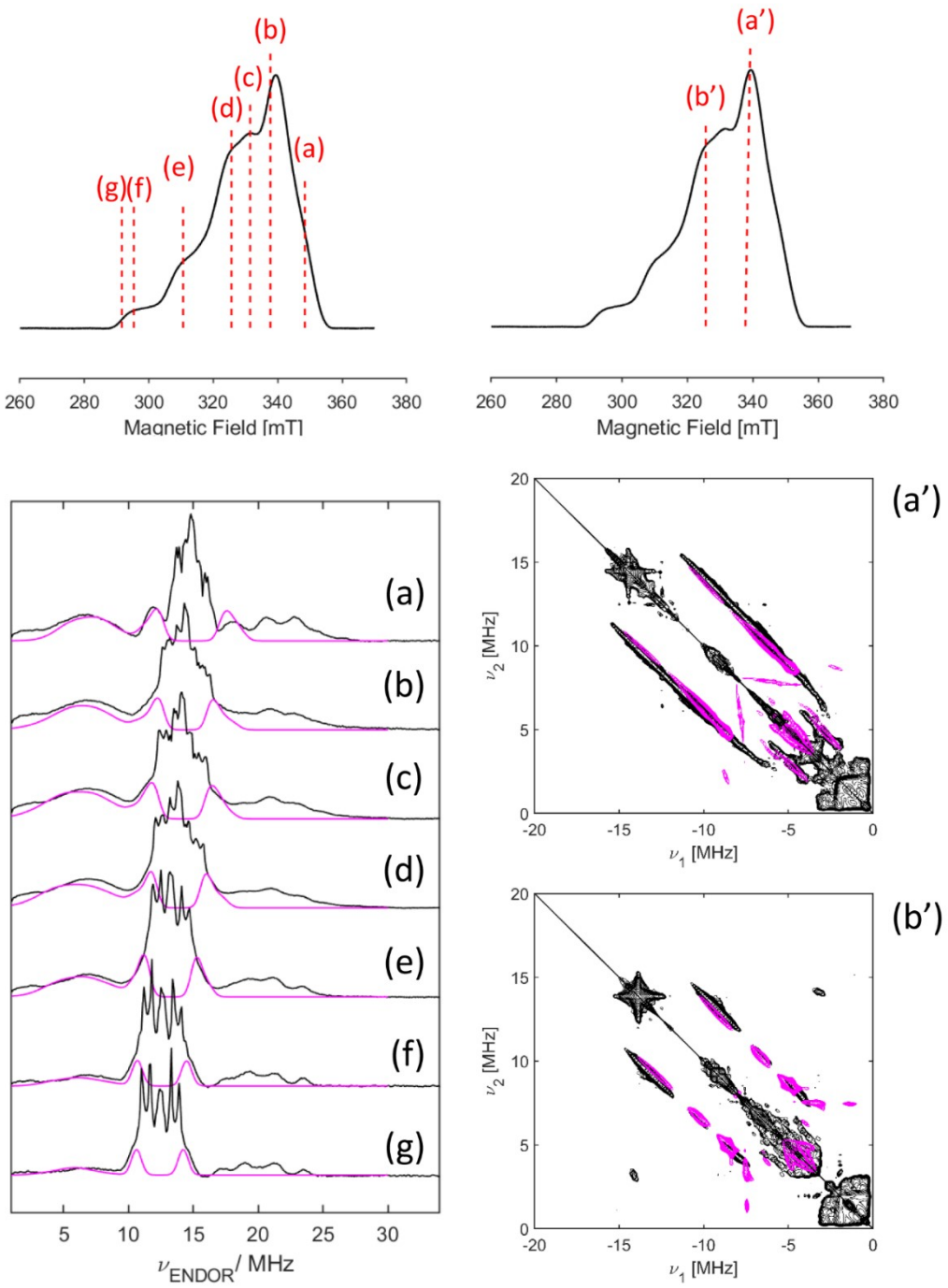

Figure S39. (left) Experimental (black) and simulated (magenta) Mims ENDOR spectra of a frozen solution of Cu(II)-PydiHis at pH 12.0 (1:1 Cu:L). Observer positions are: (a) 348.4 mT, (b) 337.7 mT, (c) 331.4 mT, (d) 325.6 mT, (e) 310.6 mT, (f) 295.3 mT, (g) 291.6 mT as indicated in the top ESE-detected EPR spectrum. The simulation include the contribution of protons H_a and H_b and the His N_δ.
(right) Experimental (black) and simulated (magenta) ^{14}N HYSCORE spectra of a frozen solution of Cu(II)-PydiHis at pH 12 (1:1 Cu:L). Observer positions are: (a') 339.2 mT and (b') 325.6 mT as indicated in the top ESE-detected EPR spectrum. The simulation includes only the contribution of the His N_δ with parameters given in Table S15.

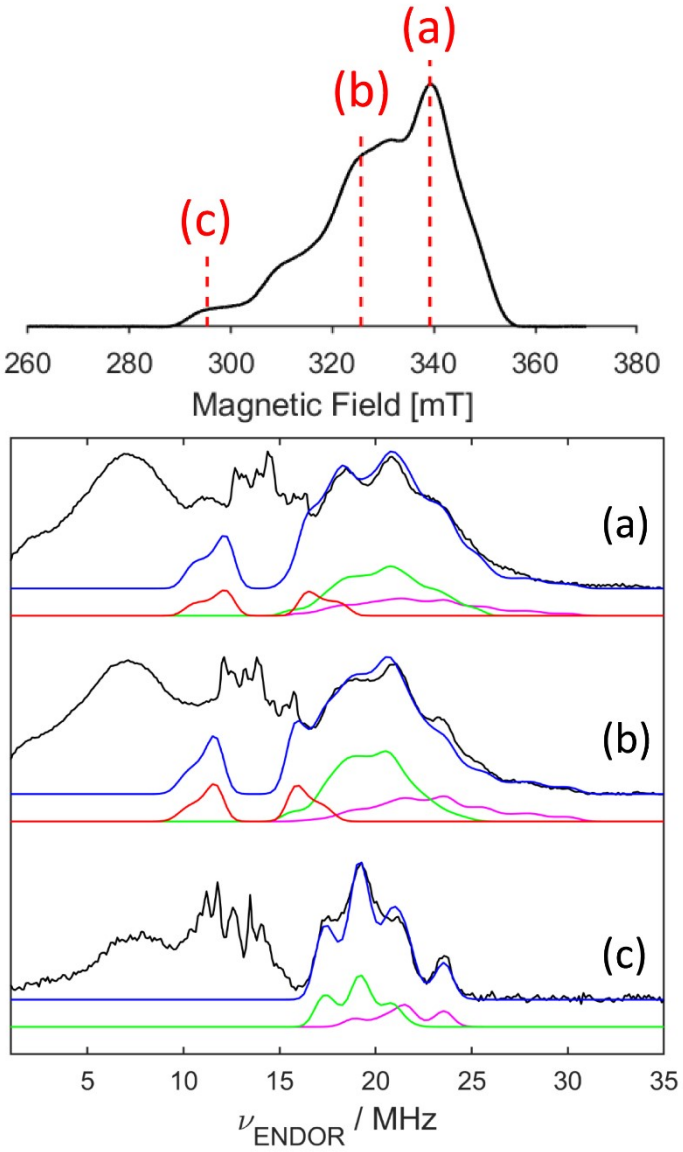

Figure S40. Experimental (black) and simulated (blue) Davies ENDOR spectra of a frozen solution of Cu(II)-PydiHis at pH 12.0 (1:1 Cu:L). Observer positions are: (a) 351.1 mT, (b) 325.6 mT, (c) 295.3 mT as indicated in the top ESE-detected EPR spectrum. The simulations contain the contributions of the H_a and H_b protons (red), the pyridine ^{14}N (magenta) and the amide ^{14}N (green). The simulation values are given in Table S14.

S9. *In vivo* studies

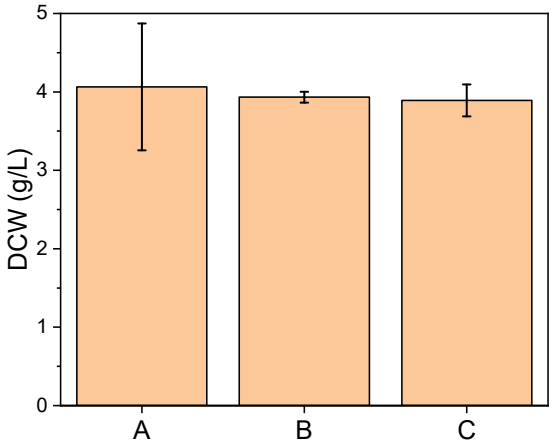

Figure S41. Effect of copper complexes on fungal biomass formation (measured as DCW). Complexes were added to the cultures at the onset of cultivations at 100 µM concentration. Samples were taken after 90 hours of incubation. **A**: control without complex; 4.1 g/L ± 0.8 **B**: 100 µM Cu(II)-PyHis; 3.93 g/L ± 0.07, **C**: 100 µM Cu(II)-PydiHis; 3.9 g/L ± 0.2.

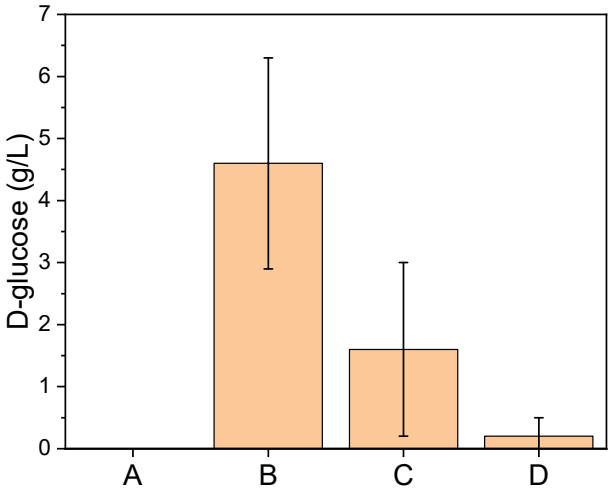

Figure S42. D-glucose concentrations (g/L) at 90 h with standard deviations.

Table S16. D-glucose concentrations (g/L) at 90 h with standard deviations (Figure S42).

Treatment group	D-glucose (g/L)
A	0 ± 0
B	4.6 ± 1.7
C	1.6 ± 1.4
D	0.2 ± 0.3

A: Control (unstressed conditions), **B**: Cells treated with 4.56 mM tBHP at 38 hours, **C**: Cells pre-incubated with copper(II) complex of PyHis (100 µM) and treated with 4.56 mM tBHP at 38 hours, **D**: Cells pre-incubated with copper(II) complex of PydiHis (100 µM) and treated with 4.56 mM tBHP at 38 hours.

Table S17. Fungal biomass (DCW) values (g/L) at 90 h with standard deviations (Figure 8, main text).

Treatment Group	100 µM	500 µM
A	4.1 ± 0.1	4.20 ± 0.04
B	0.6 ± 0.1	1.0 ± 0.3
C	0.9 ± 0.2	1.5 ± 0.7
D	0.6 ± 0.4	2.4 ± 1.0

A: Control (unstressed conditions), **B**: Cells treated with 4.56 mM tBHP at 38 hours, **C**: Cells pre-incubated with copper(II) complex of PyHis and treated with 4.56 mM tBHP at 38 hours, **D**: Cells pre-incubated with copper(II) complex of PydiHis and treated with 4.56 mM tBHP at 38 hours.

References

1. D. C. Crans, L. Yang, T. Jakusch and T. Kiss, Aqueous Chemistry of Ammonium (Dipicolinato)oxovanadate(V): The First Organic Vanadium(V) Insulin-Mimetic Compound, *Inorganic Chemistry*, 2000, **39**, 4409-4416.
2. B. J. Hathaway and D. E. Billing, The electronic properties and stereochemistry of mono-nuclear complexes of the copper(II) ion, *Coordination Chemistry Reviews*, 1970, **5**, 143-207.
3. L. Husáriková, Z. Repická, J. Moncol, D. Valigura, M. Valko and M. Mazúr, Unusual EPR Spectra with Inverse Axial g values of Chlorosalicylate–Cu(II)–2,6-Pyridinedimethanol Complex in Frozen Water–Methanol Solution, *Applied Magnetic Resonance*, 2013, **44**, 571-582.
4. J. Haak, O. Golten, M. Sørlie, V. G. H. Eijsink and G. E. Cutsail, pH-mediated manipulation of the histidine brace in LPMOs and generation of a tri-anionic variant, investigated by EPR, ENDOR, ESEEM and HYSCORE spectroscopy, *Chemical Science*, 2025, **16**, 233-254.
5. I. Sóvágó, T. Kiss and A. Gergely, Effect of mixed-ligand complex formation on the ionization of the pyrrole hydrogens of histamine and histidine, *Journal of the Chemical Society, Dalton Transactions*, 1978, 964-968.
6. A. Potapov, K. M. Lancaster, J. H. Richards, H. B. Gray and D. Goldfarb, Spin Delocalization Over Type Zero Copper, *Inorganic Chemistry*, 2012, **51**, 4066-4075.
7. N.-A. Stamos, E. Ferentinos, M. Chrysina, C. P. Raptopoulou, V. Psycharis, Y. Sanakis, D. A. Pantazis, P. Kyritsis and G. Mitrikas, Unusual 31P Hyperfine Strain Effects in a Conformationally Flexible Cu(II) Complex Revealed by Two-Dimensional Pulse EPR Spectroscopy, *Inorganic Chemistry*, 2020, **59**, 3666-3676.